PERFORMANCE ANALYSIS OF SOLAR ABSORBING FLUIDS IN CHANNEL FLOW INCORPORATING SELECTIVE SURFACES

BY

OSMAN KALEEM SIDDIQUI

A Thesis Presented to the
DEANSHIP OF GRADUATE STUDIES

KING FAHD UNIVERSITY OF PETROLEUM & MINERALS

DHAHRAN, SAUDI ARABIA

In Partial Fulfillment of the
Requirements for the Degree of

MASTER OF SCIENCE

In

MECHANICAL ENGINEERING

MAY 2013

KING FAHD UNIVERSITY OF PETROLEUM & MINERALS
DHAHRAN, SAUDI ARABIA

DEANSHIP OF GRADUATE STUDIES

This thesis, written by **Osman Kaleem Siddiqui** under the direction of his thesis advisor and approved by his thesis committee, has been presented to and accepted by the Dean of Graduate Studies, in partial fulfillment of the requirements for the degree of **MASTER OF SCIENCE** in **MECHANICAL ENGINEERING**.

Thesis Committee

Thesis Advisor
Dr. Bekir Sami Yilbas

On his behalf

Department Chairman
Dr. Zuhair Mattoug Gasem

Member
Dr. Ahmet Ziyaettin Şahin

Dean of Graduate Studies
Dr. Salam Adel Zummo

Member
Dr. Shahzada Zaman Shuja

22/4/13

Date

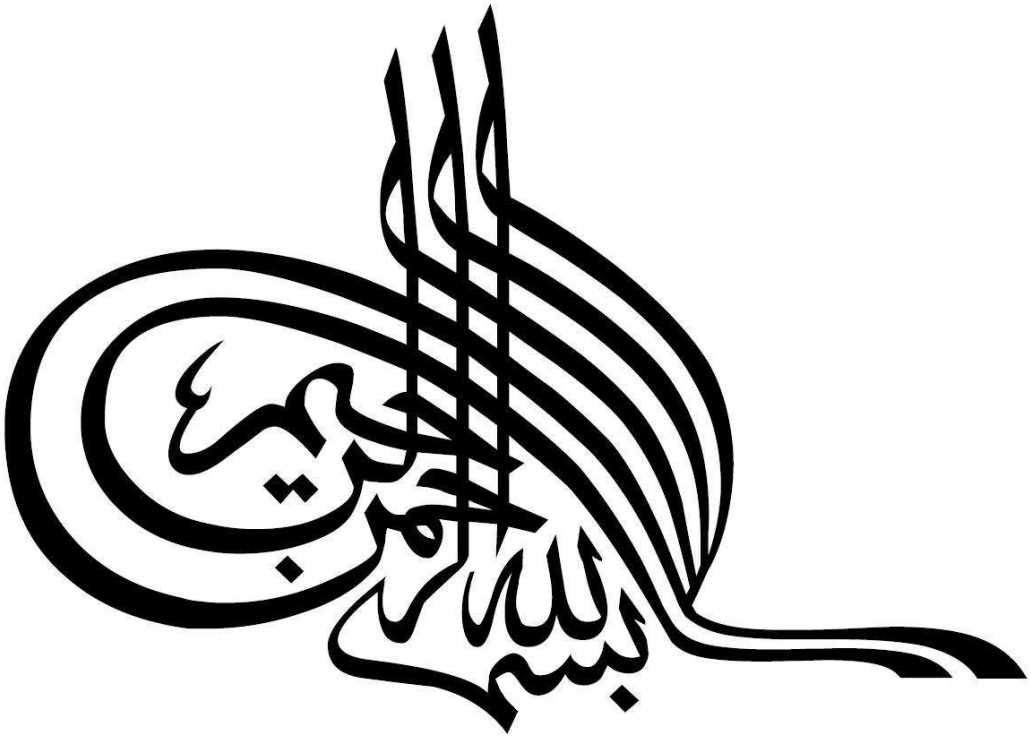

In the name of Allah,
the Most Beneficent,
the Most Merciful

Dedicated to

My mother, my father, my brothers, my sister, and all

my teachers who made this effort possible

ACKNOWLEDGEMENT

In the name of Allah, the Most Gracious, the Most Merciful.

So exalted is He, in whose hand is the realm of all things and to Him you will be returned (36:83, Al-Quran).

I begin by testifying that there is no god worthy of worship except Allah and Prophet Mohammed (peace and blessings of Allah be upon him) is his last messenger. All praise and thanks to Allah for bestowing me with health, strength, knowledge and persistence and for guiding me towards the best direction from the critical junctions of life. May Allah accept my efforts and help me in my future endeavors and grant me place in Paradise, which is the ultimate success.

I would like to acknowledge King Fahd University of Petroleum and Minerals for providing me with the facilities to accomplish my thesis objectives. I would also like to acknowledge the funded project RG 1204 via the Deanship of Scientific Research and Center of Excellence for Scientific Research Collaboration with MIT and King Fahd University of Petroleum and Minerals, Dhahran, Saudi Arabia for this work.

My deepest gratitude goes to my thesis advisor Dr. Bekir S. Yilbas, for all his support, advice and his invaluable time to guide me throughout the duration of my degree. I also appreciate his caring attitude and brotherly advices which led to my professional growth. I was immensely inspired by his hard working nature and devotion to his work. It was an honor for me to work under his guidance and to benefit from his vast experience.

I am thankful to Dr. Ahmet Sahin for his support, motivation and suggestions to improve the quality of this work. I am also grateful to Dr. Shahzada Shuja for sharing his experience in technical softwares, which was of invaluable help for me.

My heartfelt respect goes to my parents, for all their tireless efforts and struggle, in guiding me to this status. They were the source of motivation for me in pursuing higher education. I am indebted to them for their love and for always standing by my side. Special thanks to my brothers and lovely sister, for sharing all the precious moments of life with me.

I would also like to thank my cousin Dr. Mohsin Siddiqui and his family, in making my stay at KFUPM enjoyable and memorable. He was a continuous source of inspiration and motivation for me. I also appreciate all the brotherly support he provided me during the course of my degree.

I also acknowledge Usama Siddiqui, for being the heart of the Research Assistants Lab and in providing help in almost every aspect of my degree. I also appreciate all my fellow colleagues and friends who made my time in RA lab and KFUPM memorable.

TABLE OF CONTENTS

LIST OF FIGURES

LIST OF TABLES

ABSTRACT (ENGLISH)

NAME: Osman Kaleem Siddiqui

TITLE: Performance Analysis of Solar Absorbing Fluids in Channel Flow Incorporating Selective Surfaces

MAJOR FIELD: MECHANICAL ENGINEERING

DATE OF DEGREE: May 2013

Analysis of volumetric solar absorption flow system incorporating an absorber plate in channel flow is investigated. The study includes the influence of absorbing plate location on the performance characteristics and the presence of phase change particles in the carrier fluid. The absorber plate consists of Zirconium Nitrate (ZrN) coating onto a thin silver (Ag) plate. Three different configurations of the absorber plate are considered in the channel to enhance the absorption of the incident solar radiation. In order to increase the thermal storage capacity of the working fluid, phase change particles of 7% concentration is incorporated in the analysis. Lauric acid is used as phase change particles and water is considered as the carrier fluid in the channel. The study is extended to include the effects of solar concentration and the Reynolds number on the performance characteristics. A numerical scheme incorporating the full radiation heating model is used in the simulations. The performance and pump power loss parameters are introduced to assess the thermal performance of the volumetric solar absorption system.

ABSTRACT (ARABIC)

ملخص الرسالة

الاسم: عثمان كليم صديقي

عنوان الرسالة: تحليل الاداء للسوائل الممتصه للطاقة الشمسية فى قناة تدفق متضمنة أ سطح انتقائيه

التخصص: الهندسة الميكانيكية

تأريخ التخرج: مايو 2013

تم إجراء دراسة على نظام التدفق الحجمي لامتصاص الطاقة الشمسية المدمج مع لوح إمتصاص في قناة تدفق. وتشمل الدراسة تأثير موقع لوح الإمتصاص على خصائص الأداء وعلى تواجد الجزيئات الناتجة من تغير حالة المادة في السائل الناقل. ويتكون لوح الإمتصاص من الزركونيوم نترات (ZrN) مطلي فوق لوحة رقيقة من الفضة(AG) . وتم إعتبار ثلاثة تكوينات مختلفة من لوحة الإمتصاص في القناة لتعزيز امتصاص الإشعاع الشمسي الساقط. ومن أجل زيادة سعة التخزين الحراري للسائل، تم ادرج الجزيئات الناتجة من تغير حالة المادة بتركيز 7٪ في الدراسة. وتم استخدام حمض اللوريك كالجسيمات الناتجة من تغير حالة المادة و استخدم الماء كسائل ناقل في القناة. وتم توسيع الدراسة لتشمل تاثير تركيز الطاقة الشمسية ورقم رينولدز على خصائص الأداء. وتم استخدام برنامج عددي مدموج مع نموذج الإشعاع الكامل للتدفئة في المحاكاة. وتم استخدام معايير الأداء ومفقودات الطاقة من المضخة لتقييم الأداء الحراري لنظام امتصاص الطاقة الشمسية الحجمي.

CHAPTER 1

INTRODUCTION

With the ever increasing energy demands and the exhaustion of fossil fuels becoming ever more real, alternate sources of energy are being sought. However, the relatively higher efficiencies of fossil fuel power systems make alternate energy sources less feasible. Currently fossil fuelled combined cycle power plants have efficiency upto 59% [1] while for the concentrated solar power plants efficiency is around 20% [2].

Solar energy utilization is one of the viable options for renewable energy applications. The efficient harnessing of solar radiation requires proper design and operation of thermal systems. There are two methods of harvesting solar energy, solar photovoltaic and solar thermal absorption. In photovoltaic cells, the photos in the solar light are absorbed by a semi-conducting material like silicon; this creates electron-hole pairs. This creates a potential difference which acts as driving for electrons to start moving in the external circuit to lower the potential difference. The composition of solar cell allows electrons to flow only in one direction. The solar thermal absorbers absorb the solar energy in a carrier fluid (water, air, etc). This energy can be used directly in air heaters or water heaters, or this energy can be used to produce steam to run steam turbines to

generate electricity. Solar thermal cells can be of concentrating type or non-concentrating type. Flat solar collectors are non-concentrating type while concentrating type collectors include parabolic trough (cylindrical collector), parabolic dish (spherical dish) or solar tower (using heliostats). Concentrating absorbers provide high temperatures normally used for electricity generation while flat absorber cells are normally used for domestic heating needs.

1.1 Solar Absorbing Surfaces

Solar selective surfaces are being used currently for absorbing the solar radiation and then transmit the energy to the carrier fluid. The surfaces are normally opaque and don't allow solar radiation to pass to the fluid. The surface absorption increases the surface temperature, which increase the temperature difference between the carrier fluid and the surface. The high surface temperature also results in higher radiation emission loss, which is quadratic in nature. To take care of this high local surface temperature, the concept of volumetric absorption comes into consideration, whereby the surface is transparent and absorption takes place within the fluid itself. By doing so, the bulk temperature of the fluid increase while the surface temperature stays low, thus reducing the surface emission loss.

The use of solar absorbing surfaces to convert solar radiative energy into thermal energy has been the research interest for over a decade. The location of solar absorber in the thermal system is important for effective and efficient harnessing of the radiative solar energy. This is because of the fact that the absorbing surface reflects partially incoming

solar radiation and acts like a thermal source radiating some fraction of the absorbed energy. Therefore, the selective surfaces for solar radiation absorption should have low reflectivity and should be located in a thermal system where the thermal system utilizes radiating from the selective surface. Consequently, performance analysis of thermal system incorporating selective surface for solar radiation absorption while leading to improved design configuration of the solar thermal system becomes essential.

An experimental setup for volumetric absorber incorporating carbon particles suspended in different gases was made by Bertocchi et al.[3]. Estimated radiation to thermal energy conversion efficiencies surpassed 80% at the highest mass flow rates. Similar experiments were performed by Hanna et al. [4]. They conducted the experiments for highly concentrated solar energy and noted that the exit temperature of fluid exceeded the wall temperature. When air was used, the combustion of carbon particles took place, with the carbon combustion energy being 3-5% of the total energy absorbed.

The use of porous solids as volumetric solar receiver was experimented by Fend et al. [5]. They noted that high performance absorbers could lead to inhomogeneous flux distribution leading to local overheating. Also flow instabilities occurred, resulting in hot spots and destruction of receiver.

1.2 Phase Change Material (P.C.M.) Particles

The use of Phase Change Material (P.C.M.) particles for increased thermal capacity is a promising technique, whereby P.C.M. particles undergo phase change while keeping the flow temperature low as compared to flow without the P.C.M. particle suspension. The

most important property of P.C.M. particles is high latent heat of fusion. Large amount of energy is absorbed by the P.C.M. particles during the phase change from solid state to liquid state. This stored energy is then made available as needed by solidification of the particles. Thus the process of melting and solidification of the suspended particles act to keep the temperature low within the carrier fluid. Due to this energy storing ability of the particles, considerable work has been done for better understanding the phenomenon involved and implementation of the P.C.M. particles in practice applications. In order to fully utilize the latent heat of fusion of P.C.M. particles, the material selected should have the melting temperature close to the operating temperature of the system. The particles should be chemically stable in the carrier fluid while being non-toxic and non-flammable. The particles are also expected to undergo repetitive melting and solidification, thus the cyclic stability is important for practical applications. For stable flow patterns, the particles should undergo low volume changes during the phase change. Salt hydrates are corrosive with poor cyclic stability, but have high melting enthalpy per unit volume. Paraffin is non-corrosive organic material , with good thermal stability [6]. A study[7] was done in 1975, on a thermal energy storage slurry consisting of paraffin encapsulated in spherical capsules in a water carrier. The slurry storage capacity was also shown to be a factor of two higher than a water system on a per unit volume basis. However the practical application of micrometer-particles was limited owing to issues such as fouling, increased pressure drop, sedimentation and erosion. The modern advancements in material technologies has allowed the manufacturing of nanometer-sized particles, overcoming the limitations due to their reduced size[8].

1.3 Objective

The objectives of the work done in this thesis are summarized below.

i. To investigate the performance of three different arrangements for the solar selective surface absorber, for various ranges of Reynolds number and solar concentration.
ii. To incorporate the P.C.M. particles within the carrier fluid to investigate the effects on the performance of the system. Parameters like performance ratio and pressure loss parameter are introduced to evaluate the performance of the system.
iii. To investigate the affect of relatively high Reynolds number on the system's performance.

1.4 Outline

The outline of the work done in this thesis is as below.

Chapter-1 gives an introduction to the subject matter. It describes the need for research into alternate energy sources to provide for the energy demands amid expected diminishing of petroleum sources in the future. The types of absorption systems are briefly discussed with discussion on the solar absorbing surfaces. Also the objectives are defined.

Chapter-2 provides literature review into the application of absorbing surfaces and phase change particles. It presents the progress and contributions made in these fields to form basis of the current work.

Chapter-3 provides the approach used in modeling the solar energy absorbing flow system. The system is explained with the respective boundary conditions defined. The methods used in modeling the material properties are also defined.

Chapter-4 provides the method used in numerical solution of the model already discussed in chapter-3. Gird independence test is provided along with the model validation of numerical solution with results already published in the literature.

Chapter-5 provides the results and discussion of the numerical solution. It is sub-divided into three sections corresponding to each of the objective defined earlier.

Chapter-6 presents the conclusion to the work done in this thesis. The scope of future work that can be done in this field is discussed.

CHAPTER 2

LITERATURE REVIEW

The review of literature consists of three sections. First section presents the work done on solar radiation absorbing surfaces. Second section presents the literature on slurry flow with Phase Change Particles. Third section is on the selection of the selective absorbing surface

2.1 Solar Absorption Heating Systems

Considerable research studies were carried out to examine volumetric absorption systems for solar energy harvesting and energy conversion. Lenert and Wang[9] investigated nanofluid volumetric receivers for solar thermal energy conversion. They provided insights into the utilization of volumetric receivers and energy conversion for nano-fluid applications. They presented a mathematical model combined with experimental study to optimize the volumetric absorber design. They considered Therminol VP-1 as the working fluid with carbon coated cobalt nanoparticles. They developed a one-dimensional transient heat transfer model with ability to study the effects of solar concentration, the nanofluid height and optical thickness on the system performance. Their numerical results were within 20% difference with the experimental study. They

found that the efficiency of the systems increased with increasing the solar concentration and the nanofluid height. After including the power cycle efficiency, they predicted optimum system efficiencies exceeding 35 %.

Forson et al.[10] analyzed the double duct single pass solar air heater performance analysis. Their setup for the solar air heater operates at low to moderates temperature (below 60°C). Natural convection drives air through the system, with linear variation in physical properties of air. A reasonable agreement was demonstrated between the mathematical model and a full scale air heater and a small scale laboratory setup. Their model was capable of predicting the incident solar radiation, heat transfer coefficient, mean air flow rates, mean air temperature and the relative humidity at the exit of the duct. They showed that the performance of the collector could be improved with proper selection of the collector parameters and the fluid mass flow rates was the dominant factor in determining the overall efficiency of the thermal systems.

Tyagi et al.[11] examined the efficiency of a non-concentrating low temperature nanofluid based direct absorption solar collector and compared its performance with that of a typical flat-plate collector. The working fluid was water with suspended aluminum nanoparticles. They developed a two-dimensional heat transfer analysis in which direct sunlight was incident on a thin flowing film of nanofluid. The effects of absorption and scattering within the nanofluid were accounted for the energy balance equation and heat transport equation were solved numerically, to temperature profile and intensity distribution within the nanofluid. They observed that the presence of nanoparticles

increases the absorption of incident radiation by more than nine times over that of pure water. According to the results obtained from this study, the efficiency of a direct absorption solar collector using nanofluid as the working fluid was found to be up to 10% higher than that of a flat-plate collector.

Nwosu[12] carried out energy optimization in design of absorber in a solar air heater using fins. He adopted exergy optimization philosophy to optimize the maximum quantity of heat transferred by the fins while generating the least entropy to conserve exergy. He showed that high efficiency of the fin improves the heat absorption and dissipation potential of a solar air heater. The possibility of reducing useful energy waste by the application of an absorptive coating has been shown.

Veeraragavan et al.[13] introduced analytical model for the design of volumetric solar flow receivers. Their model includes the investigation of the effect of heat loss, particle loading, solar concentration and channel height on receiver efficiency. The analytical model was formulated by modeling the absorption of solar radiation by the suspended nanoparticles as a volumetric heat release inside the flowing heat transfer fluid. The energy equation was solved with the surface heat losses modeled using a combined radiative and convective heat loss coefficient. The heat transfer fluid considered was Therminol VP-1 with suspended graphite particles in 1 cm deep channel with solar concentration of 10. They predicted an optimum total system efficiency of 0.35 for a dimensionless receiver length of 0.86. The analytical model was also used to estimate the

optimum efficiency and the corresponding optimum receiver length for different design configurations.

Alvarez et al.[14] designed and tested a single glass air solar collector with the absorber plate made of recyclable aluminum can. The cans were blackened with common opaque paint having absorptance 0.903 and reflectance 0.097. A simulation model was implemented to determine the design parameters, with the configuration being found by a hydrodynamic numerical study. The resulting thermal efficiency was in agreement with the reported ones. They showed that the efficiency increase of air solar collector using recyclable aluminum cans is technically and economically feasible provided due consideration is given to the design. The recyclable cans reduce the cost of the absorber and are environmentally clean.

Wu et al.[15] introduced the coupled radiation and flow modeling in volumetric solar receivers. They used ceramic foams as absorbing material in volumetric solar air receiver in concentrated thermal power receivers. They analyzed the temperature distribution within the fluid and solid domains. They included the pressure drop associated with foam filled receiver and the interfacial heat transfer between the foam and the flowing fluid. They used P1 approximation to solve the radiative heat transfer equation within the system. Their model shows good agreement with the experimental results. Based on their model, sensitivity analysis was conducted to analyze the effect of various parameters like velocity, porosity, mean cell size and thermal conductivity of the foam on the temperature profiles. The findings revealed that the thermal non-equilibrium phenomena

were locally important and the mean cell size had dominant effect on the temperature field.

Hegazy[16] examined the performance of solar air heaters incorporating constant/variable flow situations. His study looks into the applicability of the analytical criterion model used for conventional systems to other flat type configurations. He assessed two basic types of air heater with flow over the absorber and on its both sides. Wide range of channel depth-to-length rations are used to analytically determine the heater performance, with the optimized ratio determined. He also investigated the effects of air flow rate, emissivity of plates and the heat loss coefficient. He indicated that channel depth to length ratio was one of the important parameters influencing the performance of the solar heaters.

Dhiman et al.[17] investigated analytically the thermal performance of a parallel flow packed bed solar heater. An analytical model was presented, to determine the temperature and heat transfer characteristics. They studied the effect of mass flow rate and porosity of the material on the thermal performance. Iterative numerical code was used to solve the combined mass and heat transfer equations. They found reasonable agreement (9.2% average error) of their results with the experimental results. They found 10-12% increase in thermal efficacy as compared to conventional non-porous air heater. They showed that the fraction of mass flow rate in the respective channels was dominant parameter in determining the thermal efficiency of the heater.

Sun et al.[18] examined the influence of channel depth on the performance of solar receiver. They used computational fluid dynamics simulations to study the effect of the channel depth on the energy gain. Both laminar and turbulent flow models were used. They showed that with the selective coating, the absorber plate should be located further away from the cover glazing to prevent excessive convective heat loss, with separation being no less than 20mm. The optimal channel depth was suggested as 10mm. Also the up channel depth ratio to down channel ratio should not be less than 1. Smaller channel depth results in significant friction loss, while larger depth increases heat loss.

Promvonge et al. [19] examined thermal behavior of a solar heater channel fitted with combined rib and delta-winglet structures. Measurements are carried out in the rectangular channel of aspect ratio 10 and height=30mm. They showed that Nusselt number and friction factor were reduced when delta-winglet combined with rib arrangement was used.

Ozgen et al.[20] investigated the thermal performance of double-flow flat-plate solar receiver with absorbing plate made of aluminum cans. This enhanced the heat transfer coefficient between the absorber plate and air. A single 4mm glass cover is used to reduce the convective and also radiative losses to the atmosphere. They experimented with three configurations, zig zag staggeration, arrangement in order and flat plate absorber. . They indicated that their findings agreed well with those presented in the open literature and the collector efficiency was improved through increasing fluid velocity (0.05kg/s).

2.2 P.C.M. Slurry Flow

In the past two decades, significant efforts have been focused on the use of phase change material to increase the thermal performance of the solar absorber system

Colvin et al.[21] investigated the enhancements in thermal capacitance and heat transfer coefficients by the use of microencapsulated phase change materials using water as the carrier fluid. They studied the effect of transient surges of heat in electronic components with applications in avionics and spacecrafts. They report doubling of the heat transfer coefficient with the use of Microencapsulated P.C.M.

Roy and Sengupta [22] presented experimental study on microencapsulated P.C.M. for the evaluation of their properties. They found that microcapsules with wall thickness of 30% of total volume are thermally and structurally stable for at least 100 cycles of phase change. They found some deterioration of the thermal properties of the particles but concluded that the P.C.M. microcapsules can be used in practical heat transfer systems.

Goel et al. [23] conducted an experimental study for the evaluation of the heat transfer characteristics of a slurry containing n-eicosane microcapsules in water. They studied laminar fully developed flow in circular duct with uniform constant heat flux. They also studied the effect of particle diameter and degree of homogeneity of the suspension. Their experimental results showed up to 50% reduction in wall temperature as compared to single phase fluid. 15% reduction in wall temperature occurred by increasing the particle diameter by a factor of 2.5.

Charunyakorn et al. [24] provided a numerical study to determine the heat transfer characteristics of microencapsulated P.C.M. slurry in circular ducts. They took into consideration both the thermal conductivity enhancement due to particle motion and the latent heat of fusion. Their results show that P.C.M. slurry can sustain the fluid temperature by enhancing the heat transfer coefficient. They reported that for the low temperature applications, heat flux 2-4 times higher may be achieved that the single phase flow

Choi et al. [25] provided an explanation of the physical mechanism, by which the P.C.M. particles enhance the convective heat transfer. They performed experiments on a circular tube with length 627 times the diameter, heated by a uniform heat flux. The working fluid was P.C.M.-Water slurry in turbulent flow. They introduced an emulsifier within the flow loop for the generation of very fine P.C.M. particles (~ 0.1mm).

Zhang and Faghri [26] conducted a numerical study of microencapsulated P.C.M. slurry in a circular tube under laminar forced convection and constant wall heat flux. A temperature transforming model is used to model the phase change inside the microcapsule. They considered the effect of initial sub-cooling and microcapsule's crust and a better agreement with the experimental results was obtained. Their results also showed that by increasing the phase change temperature range, the effect of the microcapsules on the forced convection heat transfer can be reduced significantly.

Roy and Avanic [27] experimentally compared the microencapsulated P.C.M. slurry with P.C.M. emulsions and found similar results. They confirmed that the microcapsule wall

does not affect the heat transfer process significantly. These results were based on study conducted laminar forced convection conditions in a circular pipe. They studied n-octadecane in water with up to 30% volume concentration.

Alisetti and Roy [28] numerically studied the convective heat transfer of P.C.M. slurries with constant wall temperatures in circular ducts. They used a homogeneous model with effective specific heat method to model the phase change of the particles. They compared different specific heat profile and found that the impact on the final solution was less than 4%.

Yamagishi et al. [29] conducted study on the heat transfer enhancement using micro-encapsulated P.C.M. in a circular tube. They studied both laminar and turbulent flows with uniform heat flux applied to the tube. They used particles of n-octadecane with up to 30% volume concentration. They found that the flow regime changes from turbulent to laminar with increase in particle volume concentration. The local heat transfer coefficient was found to increase with increasing degree of turbulence, heating rate in tube and the particle volume concentration.

Roy and Avanic [30] conducted a numerical study using homogeneous model, with effective specific heat approach for modeling phase change. A fully developed inlet condition was given with constant heat flux applied to the tube. They developed a correlation for prediction of wall temperature rise as a function of the axial length.

Hu and Zhang [31] numerically studied convective heat transfer enhancement with microencapsulated P.C.M. slurry in a circular tube subjected to a constant heat flux.

They used a homogeneous model for solving the fluid flow and heat transfer of the P.C.M. slurry in the tube. The melting of P.C.M. particle was modeled using the effective specific heat method. They compared four different specific heat functions for modeling the phase change of P.C.M. particles within the melting range and reported that the knowledge of exact nature of phase change process is more important in the thermal entry region. The degree of enhancement in heat transfer is greater in thermally fully developed region as compared to thermal entry region. Increase in bulk Reynolds number was also found to increase heat transfer significantly for a given fluid.

Awad et al. [32] studied heat transfer enhancement in a micro-channel flow with a presence of phase change particles in a carrier fluid. They demonstrated that the Nusselt number increased significantly in the wall region because of the phase change particles in the flow system.

2.3 Selective Surface

A selective surface [33] is one that has high absorptance and low emittance, thus has the ability to harness the solar energy effectively while limiting the losses due to emission. For spectrally selective surface, the lower wavelength solar radiation is absorbed and low surface emission occurs of the higher wavelength. Cutoff wavelength is the wavelength below which the absorption is high and above it emission is low. The cutoff wavelength is preferred to be 2 μm as most of the solar radiation lie below this wavelength and low temperature surface emission lies above 2 μm wavelength.

There are several criterion used for evaluating the solar selective surface. Ideally the absorptance is limited to 0.99 while the emittance is limited to 0.01. Any surface near these values is considered good. Ratio of absorptance to emittance also provides information about degree of selectivity. For non-selective surface, the ratio is 1. For ideal selective surface, the ratio is 99. Any surface with ratio greater than 10 is considered good. The best indicator to determine the usefulness of solar selective surface is the conversion efficiency, CE. It is defined as[34]

$$CE = \frac{Q_a - Q_e}{Q_s}$$

Where Q_a is the absorbed solar flux, Q_e is the emitted solar flux and Q_s is the incoming solar flux.

Zirconium Nitride coating, 0.16μm thick, on Silver (ZrN–Ag) tends to follow good pattern for selective surface having transition wavelength centered a 2 μm. It has absorptance of 0.86 and emittance of 0.039 at 600K, with conversion efficiency of 0.52 [33].

In the present study, the thermal performance of solar heater system incorporating the selective surface in a channel is investigated. Influence of location of absorbing plate and the flow Reynolds number on the performance characteristics of the flow system is analyzed. Water is used as a working fluid and numerical scheme incorporating radiation absorption and emission is adapted for the thermal and flow analysis

CHAPTER 3

THE MODEL STUDY

This chapter contains the detailed information about the models used for formulating the fluid flow, radiative heat transfer and P.C.M. particles. The first section presents the mathematical model for single phase fluid flow. The second section gives information about the Discrete Ordinates Radiation model. The third section presents the mathematical treatment of the PCM slurry. In the fourth section, the problem definition and the boundary conditions are defined.

3.1 Single phase model

The governing equations used for the single phase model are continuity, momentum and energy equation with an additional radiative transfer equation to model the radiation heat transfer. The equations are shown below:

Continuity equation

$$\nabla \cdot \vec{v} = 0 \tag{3.1.1}$$

Momentum equation

$$\nabla \cdot \left(\rho \vec{v}\vec{v} \right) = -\nabla p + \mu \nabla^2 v \tag{3.1.2}$$

Energy equation

$$\nabla \cdot \left(\vec{v} \left(\rho c_p T \right) \right) = \nabla \cdot \left(k \nabla T \right) + S \tag{3.1.3}$$

where v is the carrier fluid velocity, ρ is the carrier fluid density, p is the pressure, μ is the carrier fluid viscosity. E represents the energy per unit mass, k represents the carrier fluid thermal conductivity, T is the temperature of the carrier fluid and S represents the energy source which is obtained from the solution of the radiative transfer equation solved in Discrete Ordinates Radiation Model.

3.2 Discrete Ordinates (DO) Radiation model

In Discrete Ordinates Radiation Model, the radiative transfer equation (RTE) is solved for finite number of discrete solid angles, determined by the angular discretization. Each solid angle is associated with a vector direction $\vec{s}$, which is fixed in relation to the global cartesian system (x, y, z). The radiative transfer equation is transformed into a transport equation, determining the radiation intensity in the spatial cartesian system (x, y, z). The radiative transfer equation is then iteratively solved for each of the solid angles.

$$\nabla \cdot (I(\vec{r}, \vec{s})\vec{s}) + a.I(\vec{r}, \vec{s}) = a.n^2 . \frac{\sigma T^4}{\pi} \tag{3.2.1}$$

Where I is the radiation intensity, which depends on position $\vec{r}$ and direction $\vec{s}$, a is the absorption coefficient, n is the refractive index, σ is the Stefan-Boltzmann constant and T is the local temperature.

The uncoupled implementation of DO model is used, which is suitable for low optical thicknesses, in the uncoupled implementation, equations for the energy and radiation intensities are solved one by one, assuming prevailing values for other variables. [35]

Figure 3.1 shows the nomenclature used for angular discretization of the spatial location. The angles θ and ϕ are the polar and azimuth angles respectively. Each octant of the angular space 4π at any spatial location is discretized into $N_\theta * N_\phi$ solid angles, with only four octants being solved in two-dimensional calculations due to symmetry.

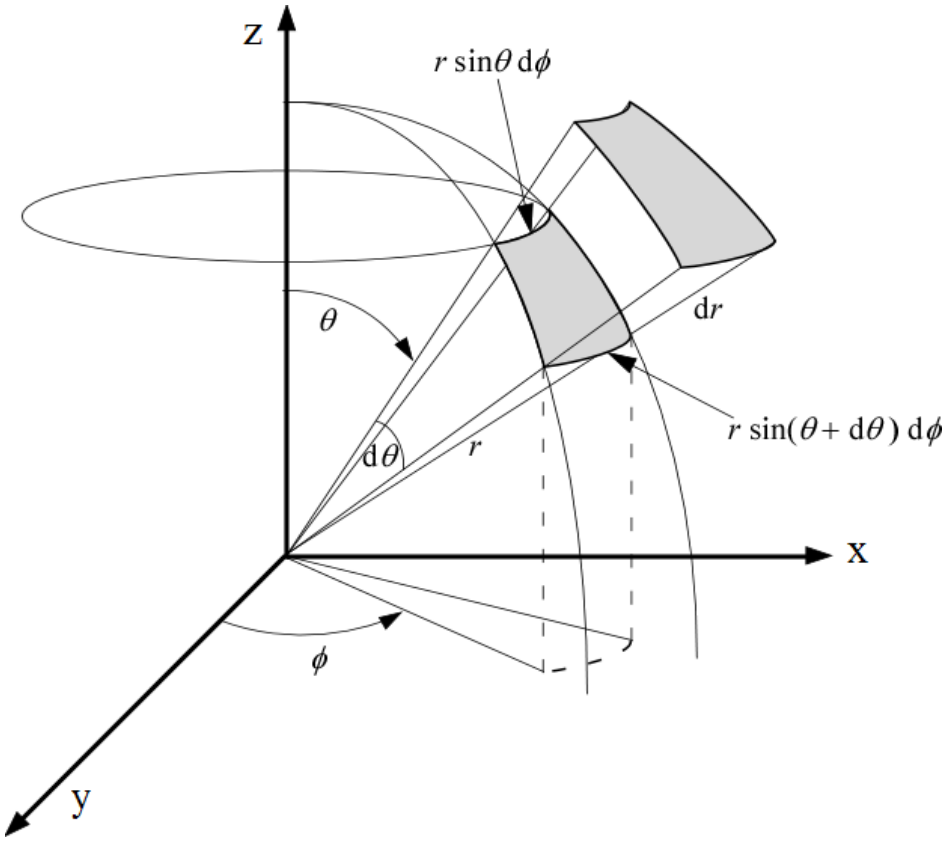

Figure 3.1. The Nomenclature for definition of Solid angles

3.2.1. Boundary Treatment for Opaque Wall

Opaque wall boundary condition takes into consideration the emission from the wall with part of the incoming radiation on the wall being absorbed and the remaining radiation reflected back.

Figure 3.2 shows the boundary treatment for the opaque wall. The incident radiation q_{in} is reflected diffusely and specularly, depending on the diffuse fraction f_d

The radiation quantities computed at the opaque boundary are as follows

Emission from the wall surface $= n^2 \varepsilon_w \sigma T_w^4$ (3.2.2)

Diffusely reflected energy $= f_d (1-\varepsilon_w) q_{in}$ (3.2.3)

Specularly reflected energy $= (1- f_d) q_{in}$ (3.2.4)

Absorption at the wall surface $= f_d \varepsilon_w q_{in}$ (3.2.5)

Where f_d is the diffuse fraction, n is the refractive index of the adjacent medium, ε_w is the wall emissivity, σ is Boltzmann's constant, and T_w is the wall temperature.

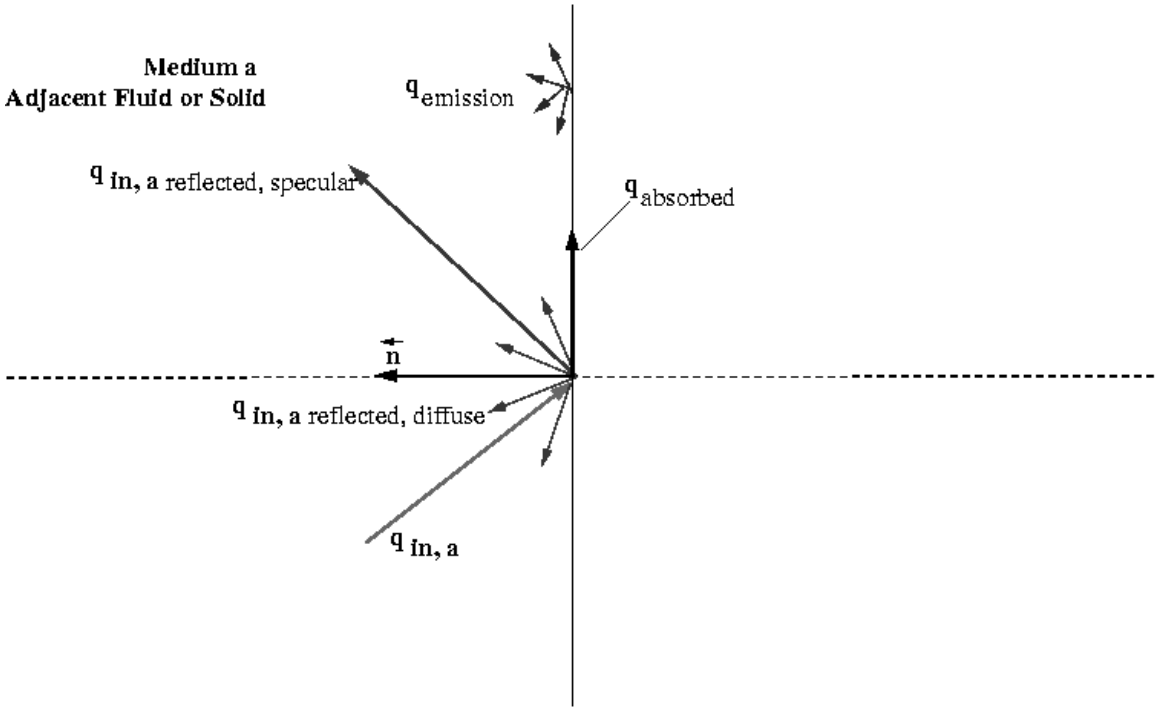

Figure 3.2. Boundary treatment for Opaque Wall [35]

3.2.2 Boundary Treatment for Semi transparent Wall

Absorption within a semi transparent wall is not taken into consideration owing to zero thickness of the wall. For absorption within the wall, solid cells are to be used to explicitly, modeling the thickness. The interface reflectivity at semi transparent wall is based on Fresnel equation. The transmitted radiation is refracted depending on the refractive index following Snell's law.

Figure 3.3 shows a graphical representation of Snell's law. A ray traveling from a semi-transparent medium *a* with refractive index n_a to a semi-transparent medium b with a refractive index n_b in the direction $\vec{s}$ is shown. Surface *a* of the interface is the side that faces medium *a*, similarly, surface b faces medium *b*. The interface normal $\vec{n}$ is assumed to point into side *a*.

A part of the energy incident on the interface is reflected, and the rest is transmitted. The reflection is specular, so that the direction of reflected radiation is given by

$$\vec{s_r} = \vec{s} - 2(\vec{s}.\vec{n})\vec{n} \tag{3.2.6}$$

The radiation transmitted from medium *a* to medium *b* undergoes refraction. The direction of the transmitted energy, $\vec{s}_t$, is given by Snell's law:

$$\sin\theta_b = \frac{n_a}{n_b}\sin\theta_a \tag{3.2.7}$$

where θ_a is the angle of incidence and θ_b is the angle of transmission,

The interface reflectivity on side a is governed by Fresnel equation given by

$$r_a(\vec{s}) = \frac{1}{2}\left[\left(\frac{n_a \cos\theta_b - n_b \cos\theta_a}{n_a \cos\theta_b + n_b \cos\theta_a}\right)^2 + \left(\frac{n_a \cos\theta_a - n_b \cos\theta_b}{n_a \cos\theta_a + n_b \cos\theta_b}\right)^2\right] \tag{3.2.8}$$

Figure 3.4 shows the semi-transparent boundary treatment. q_{in} is the incident radiation from medium *a*, part of it is reflected with the reflectivity given by Fresnel equation (3.2.8). This reflected radiation can be diffuse or specular, based on the value of diffuse fraction f_d. The transmitted radiation undergoes refraction based on Snell's law. The diffusive behavior of transmitted radiation is controlled by the diffuse fraction f_d.

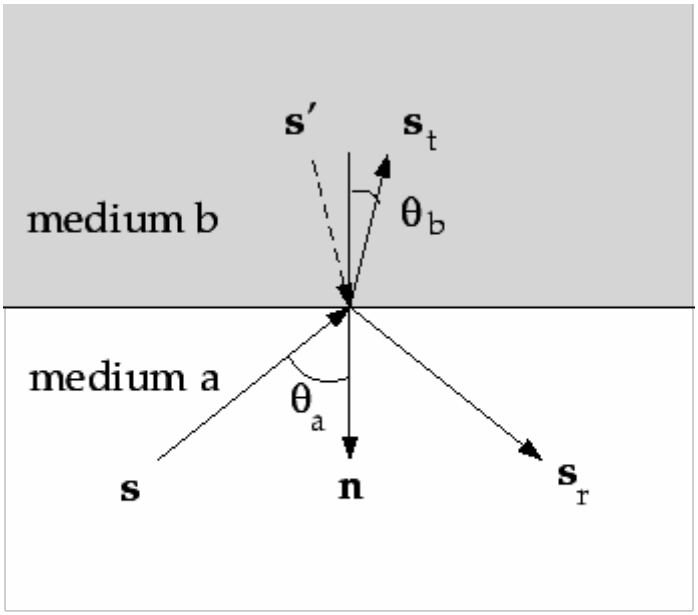

Figure 3.3. Reflection and Refraction of Radiation at the Interface Between Two Semi-Transparent Media [35]

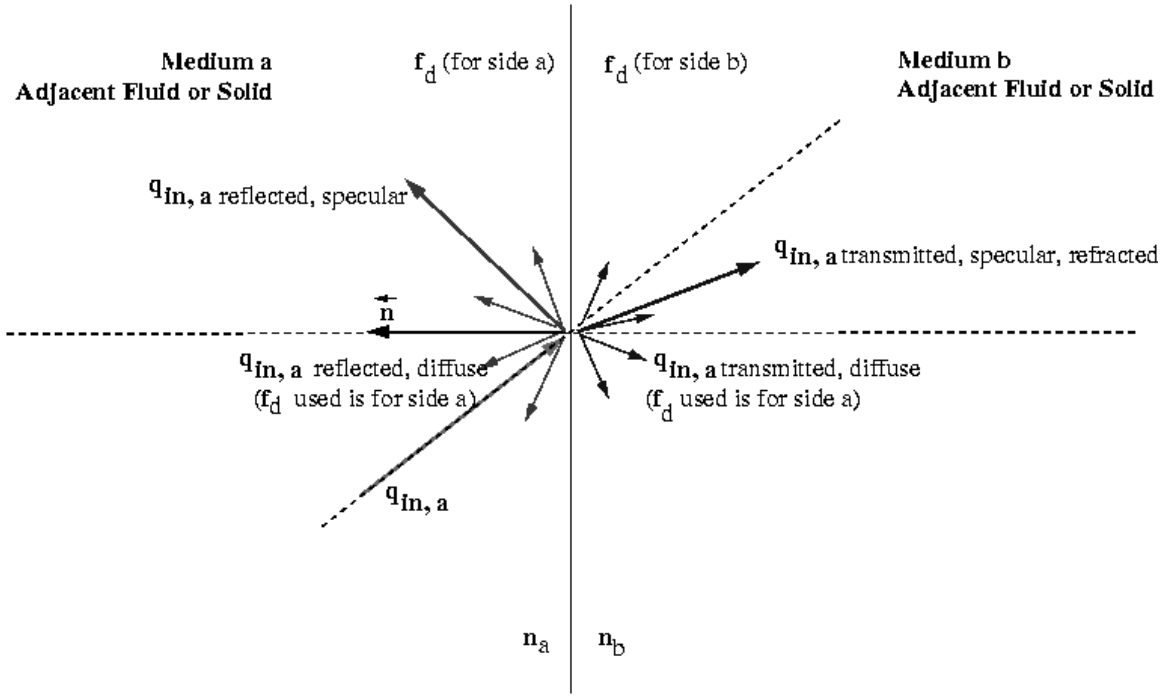

Figure 3.4. Boundary treatment for Semi transparent Wall [35]

3.3 Modelling Phase Change Particles

The homogeneous model is used to model the P.C.M. particles. This unified model was found to effectively model the P.C.M. particles by A.B.S. Alquaity[36]. In this model the perticles and carrier fluid are assumed to have the same temperature and velocity. Effective thermo-physical properties are used to solve the governing equations of mass, momentum and energy.

1. The flow in the channel is steady and laminar
2. The particles are distributed homogeneously inside the channel.
3. The bulk fluid is Newtonian.
4. The phase change of particles occur between the solidus and liquidus temperatures.

The governing equations for the homogenous model with effective properites are shown below.

Continuity equation

$$\nabla \cdot \vec{v} = 0 \tag{3.3.1}$$

Momentum equation

$$\nabla \cdot \left(\rho_b \vec{v}\vec{v} \right) = -\nabla p + \mu_b \nabla^2 v + \vec{F} \tag{3.3.2}$$

Energy equation

$$\nabla \cdot \left(\rho_b \vec{v} c_{pb} T \right) = \nabla \cdot \left(k_b \nabla T \right) + S \tag{3.3.3}$$

where *v* is the bulk fluid velocity, ρ_b is the bulk fluid density, *p* is the pressure, and μ_b is the viscosity of the bulk fluid. In the above equation C_{pb} represents the bulk fluid specific heat, k_b is the bulk fluid thermal conductivity and *T* is the temperature of the bulk fluid. The calculation of the thermo-physical properties are based on the models discussed in the proceeding section.

3.3.1 Bulk Fluid Thermo-Physical Properties

Following models are used for the calculation of the effective thermo-physical properties of the bulk fluid (combined carrier fluid with P.C.M. particles)

3.3.1.1 Density

The density of the bulk fluid is calculated using mass balance

$$\rho_b = c\rho_p + (1-c)\rho_f \tag{3.3.4}$$

where ρ_p is the density of the particles and ρ_f is the carrier fluid density.

3.3.1.2 Thermal conductivity

Maxwell's model is used for the calculation of effective thermal conductivity of the bulk fluid. The bulk thermal conductivity using Maxwell's model[37] is calculated as

$$k_b = k_f \frac{2 + k_p/k_f + 2c\left(k_p/k_f - 1\right)}{2 + k_p/k_f - c\left(k_p/k_f - 1\right)} \tag{3.3.5}$$

3.3.1.3 Viscosity

The introduction of P.C.M. nanoparticles into the carrier fluid increases its viscosity. The calculation of bulk viscosity is based on Vand's correlation.[38] as

$$\mu_b = \left(1 - c - 1.16c^2\right)^{-2.5} \mu_f \tag{3.3.6}$$

3.3.1.4 Specific Heat

.An effective specific heat model is used to account for the phase change of the particles in the micro-channel by varying the specific heat capacity of the particles across the solidus and the liquidus temperatures. The specific heat of the bulk fluid is calculated using energy balance as [39]

For $T_p < T_{solidus}$

$$c_{pb} = \frac{c\left(\rho c_{p,S}\right)_p + (1-c)\left(\rho c_p\right)_f}{\rho_b} \tag{3.3.7}$$

For $T_{solidus} < T_p < T_{liquidus}$

$$c_{pb} = \frac{c\left(\rho\left(\frac{c_{p,S} + c_{p,L}}{2} + \frac{L_{fusion}}{T_{liquidus} - T_{solidus}}\right)\right)_p + (1-c)\left(\rho c_p\right)_f}{\rho_b} \tag{3.3.8}$$

For $T_P > T_{liquidus}$

$$c_{pb} = \frac{c\left(\rho c_{p,L}\right)_p + (1-c)\left(\rho c_p\right)_f}{\rho_b} \tag{3.3.9}$$

where $\left(c_p\right)_f$ is the specific heat of the carrier fluid, $\left(c_{p,S}\right)_p$ is the specific heat of the P.C.M. particle in solid state and $\left(c_{p,L}\right)_p$ is the specific heat of the P.C.M. particle in the liquid state.

The thermo-physical properties of water and particles are listed in Table 3.1

Table 3.1 Thermo-physical properties of P.C.M. particles and Water

	Density kg/m^3	Specific Heat kJ/kg K	Latent Heat kJ/kg	Thermal conductivity W/m K
Particle (Solid)	1007	1.76	211	0.147
Particle (Liquid)	862	2.27	-	0.147
Water	998.2	4.182	-	0.6

3.4 Geometric Configuration

Three cases are modeled in the work, with the absorbing surface in different locations. The channel height is 5 mm. The total channel length is 1.5m, with the middle 0.5m section absorbing the radiation. The remaining sections are considered to be opaque. A Zr-N coating is used on silver substrate, coating thickness is 0.16 μm and silver substrate is 0.5mm thick.

Figure 3.5 shows the case (1), the absorbing surface is placed on the irradiated side (top). The absorption takes place in the top coating and then it is conducted to the fluid.

Figure 3.6 shows the case (2), the absorption surface is placed at the bottom with a glass cover at the top surface to provide structural strength and transmit the radiation. The transmitted radiation is volumetrically absorbed in the fluid and remaining radiation gets absorbed in the coating.

Figure 3.7 shows the case (3), a semi-transparent plate is added to case (2) such that majority of the radiation is absorbed in the middle and the coating at the bottom ensures that all radiation gets absorbed.

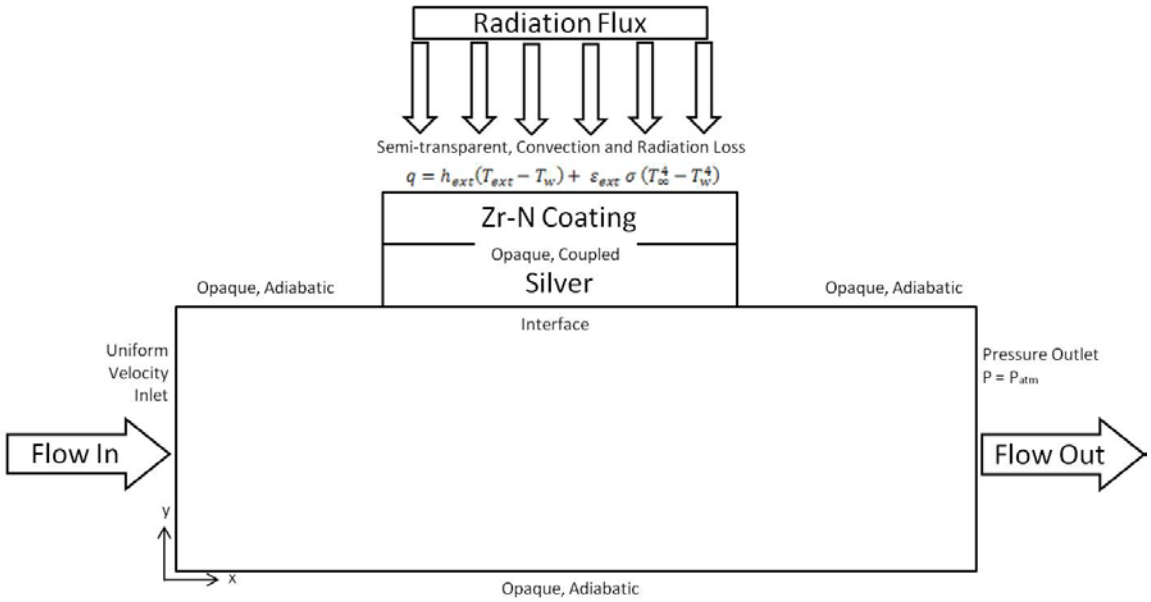

Figure 3.5. Case-1, Selective surface at top

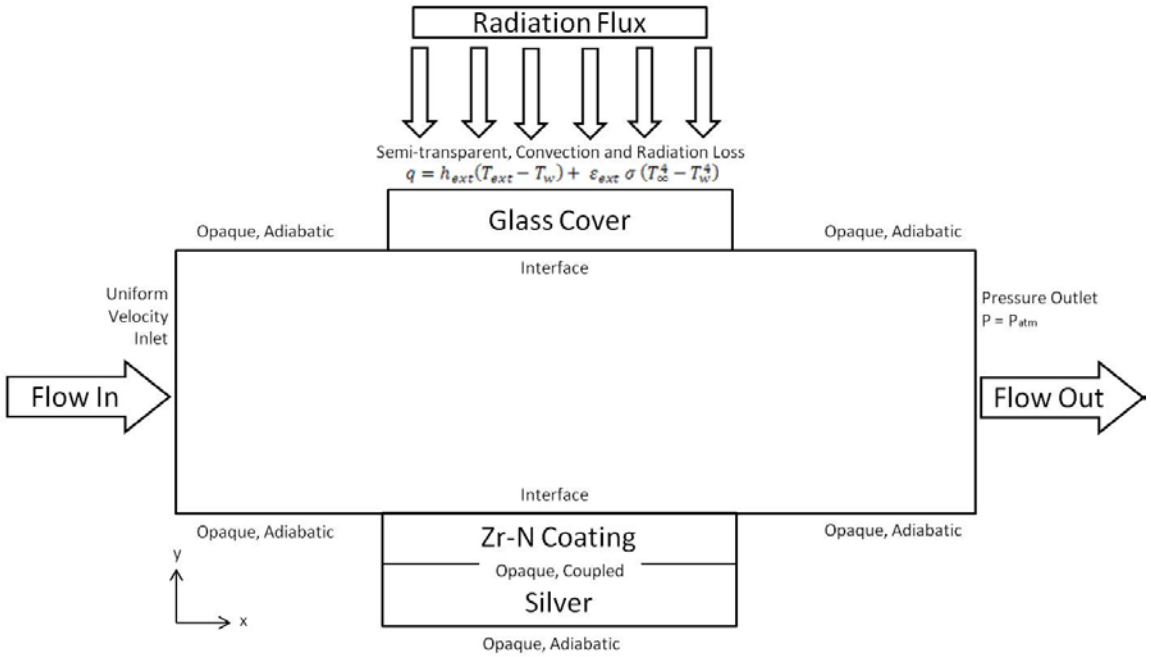

Figure 3.6. Case-2, Selective surface at bottom

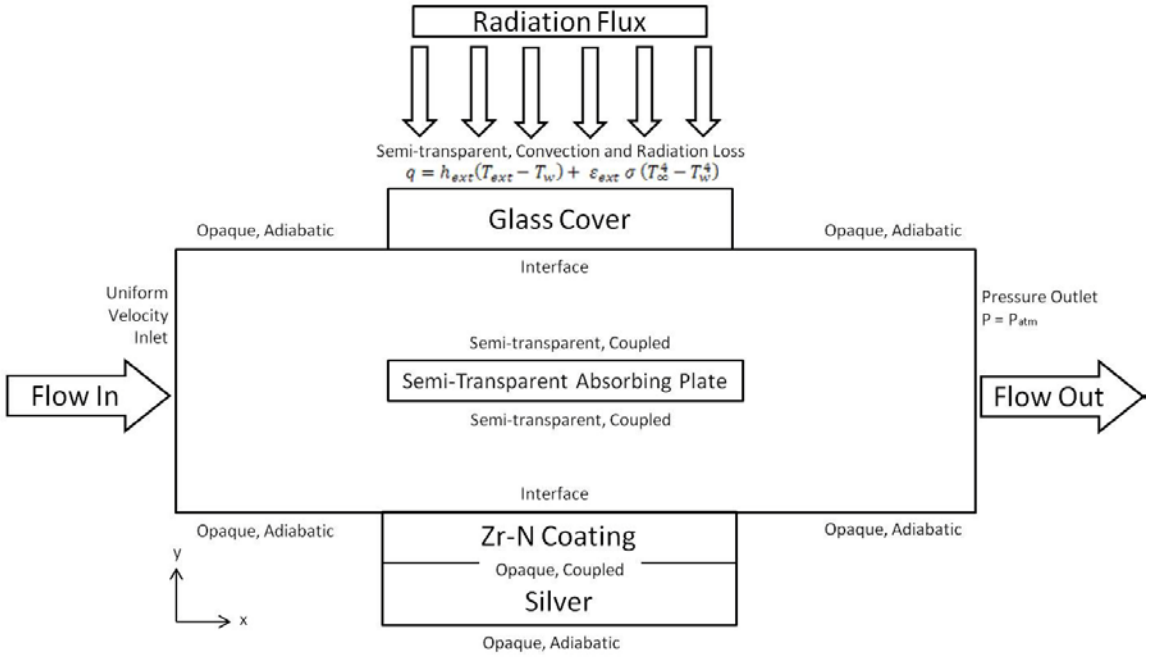

Figure 3.7. Case-3, Selective surface at bottom with mid-height semi-transparent absorber

3.5 Boundary conditions

The Boundary conditions set are discussed below

3.5.1 Inlet

A uniform velocity profile is used at the inlet. The temperature of the fluid at the inlet is specified as 315 K, lower than the melting temperature of the P.C.M. particles.

3.5.2 Outlet

At the flow exit , pressure outlet boundary condition is used which specifies a zero gauge pressure (1atm) at the outlet. The diffusion fluxes for temperature and velocity are zero in the normal direction of the exit plane.

3.5.3 Middle Top Surface

Irradiance is applied on the 0.5m top surface at the middle of the domain. This surface is defined as Semi-transparent to allow irradiance to enter the domain. A mixed Thermal boundary condition is used to model the thermal losses from the top surface. Mixed boundary condition models both convective and radiation losses to the surroundings.

3.5.4 Top Glass and Center Absorber Surface

For cases 2 and 3, both surfaces of the top glass are set as semi-transparent

For case 3, both surfaces of the absorber are also set as semi-transparent

3.5.5 Other Boundaries

Adiabatic boundary condition is applied to all remaining surfaces, such that there is no heat loss from them.

CHAPTER 4

NUMERICAL SOLUTION

Fluent^{TM} uses control volume approach to discretize the governing equations. SIMPLE scheme[40] is used for pressure-velocity coupling. The non-linear set of equations are solved using iterative method with the convergence criterion of residuals set to 10^{-6} for continuity and momentum, and 10^{-10} for energy and DO equations. In addition, surface monitors at the outlet are monitored for velocity and temperature to ensure convergence.

Due to the small thickness of the absorbing layer, non conformal meshing is used to allow for different mesh densities. Non-conformal meshing allows the cell zones to pass flux from one mesh to another even when the mesh node locations are not coinciding.

4.1 Grid Generation

Grid independence test was carried out to determine mesh convergence. The temperature profiles for the test are shown in Figure 4.1. It is evident from the Figure 4.1 that by increasing the mesh points there is insignificant variation in the values of the predicted temperature values, however by reducing the mesh points, there is a notable difference in the temperature values.

Based on the results, following mesh sizes were used:

For the fluid flow region, there are 3,000 cells in the flow direction and 30 across the flow direction.

The center absorber surface has 1,000 cell in the flow direction and 2 cells across the flow direction.

The Silver layer has 1,000 cells in the flow direction and 10 cells across the flow direction.

The Zr-N layer has 1,000 cells in the flow direction and 2 cells across the flow direction.

In Figure 4.2 , the meshed domain is shown with enlarged sections within the circles

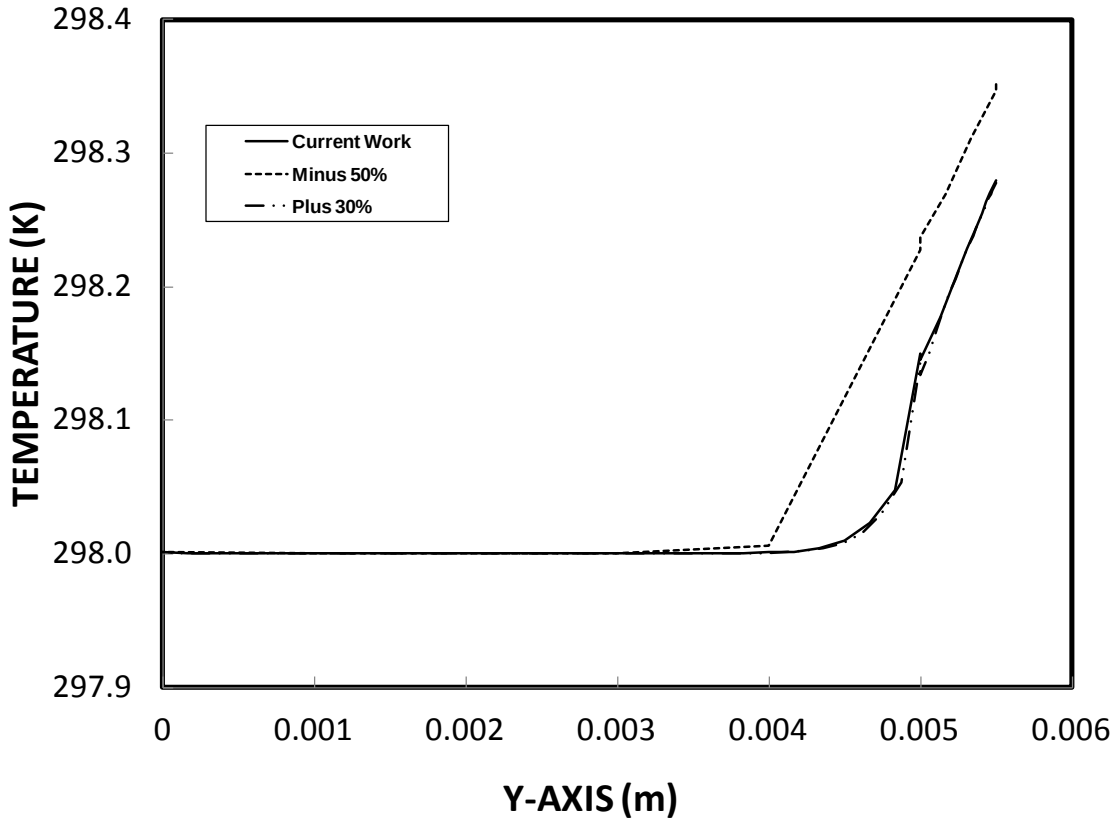

Figure 4.1. Grid independent results for temperature distribution at x = 0.5 m.

It should be noted that minus 50% corresponds to half of the mesh size used in the simulations while plus 30% represents 1.3 times of the mesh used in the simulations.

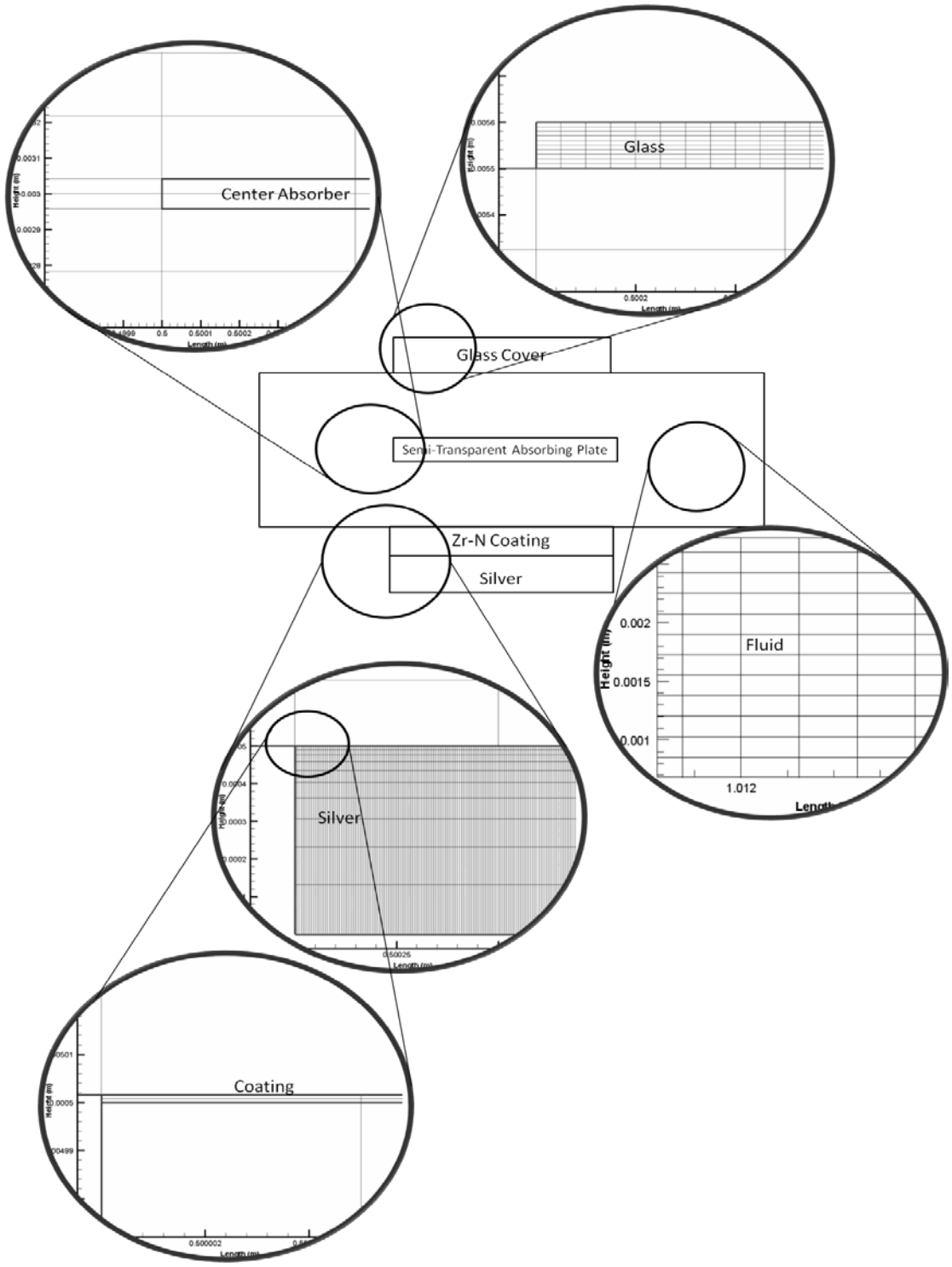

Figure 4.2. The Meshed Domain

4.2 Model Validation

In order to validate the model used in the simulations, the dimensionless temperature values are reproduced in line with the geometric configurations and the respective boundary conditions presented in the previous study by Veeraragavan et al. [13]. The identical conditions and geometry provide the comparison of dimensionless temperature data obtained from the analytical solution [13] and the model predictions. The findings are given in Table 4.1. The dimensionless length scale along the x and y-axes of the channel is incorporated in Table 4.1 are in line with the previous study [13]. The dimensionless length scale is defined as: $\overline{x} = \frac{x}{H.Pe}$ and $\overline{y} = \frac{y}{H}$, where *x* and *y* are the distances along the x and y-axes, *H* is the channel height along the y-axis, and *Pe* is the Peclet number (*Pe* = *Pr.Re*). It can be observed that the values of dimensionless temperature predicted from the present study and obtained from the previous work [13] are in good agreement. The small discrepancies can be associated with the assumption of unidirectional incidence and absorption model in the analytical solution as well as the numerical errors related to the truncation errors. Nevertheless, the discrepancies are considerably small.

	$\bar{x}$= 0.2		$\bar{x}$= 1		$\bar{x}$= 2	
$\bar{y}$	Simulation	Literature [6]	Simulation	Literature [6]	Simulation	Literature [6]
0.30	0.1866	0.2136	0.5842	0.6200	0.8167	0.8743
0.35	0.1782	0.1966	0.5832	0.6108	0.8167	0.8734
0.40	0.1697	0.1768	0.5821	0.6017	0.8166	0.8709
0.45	0.1613	0.1608	0.5810	0.5915	0.8165	0.8671
0.50	0.1531	0.1449	0.5799	0.5820	0.8163	0.8643
0.55	0.1454	0.1301	0.5789	0.5739	0.8161	0.8615
0.60	0.1382	0.1162	0.5780	0.5658	0.8160	0.8586

Table 4.1 Dimensionless temperature values predicted from the present simulations and obtained from previous study [13]

CHAPTER 5

RESULTS AND DISCUSSION

This chapter consists of three sections. In Sections 1, the performance analysis of the three absorber plate configuration is discussed. In Section 2, the influence of the presence of phase change particles in the three configurations is discussed for lower Reynolds number. In Section 3, the higher Reynolds number case is discussed.

5.1 Absorber plate configurations

In order to assess the influence of absorbing plate on the thermal performance of the channel, the performance parameters are introduced in line with the previous study [41]. The parameters are described below

The temperature ratio (ϕ), the ratio between the maximum and bulk temperatures as compared to the inlet temperature,

$$\phi = \frac{T_{max} - T_b}{T_{max} - T_{in}} \tag{5.1.1}$$

The performance parameter (E), the heat gain by the flow over the heat input by the solar radiation in the channel,

$$E = Q_{gain} / Q_{in} \tag{5.1.2}$$

where the heat input and heat gain are defined as

$$Q_{in} = C \times I \times A \tag{5.1.3}$$

$$Q_{gain} = \dot{m} \cdot C_p \cdot \left(T_{out} - T_{in}\right) \tag{5.1.4}$$

where, C is solar concentration, I is incident radiation and A is the irradiated area of the top absorber/plate

The Pump power lost parameter (h_L), pump power loss over the heat gain by the fluid in the channel.

$$h_L = h_{P,L} / Q_{gain} \tag{5.1.5}$$

where the pump power loss and the volume flow rate is calculated as

$$h_{P,L} = \dot{V} \cdot \Delta P \tag{5.1.6}$$

$$\dot{V} = \dot{m} / \rho \tag{5.1.7}$$

Where $\dot{V}$ is the volume flow rate, ΔP is pressure loss in the channel, $\dot{m}$ is the mass flow rate and ρ is the density of the fluid

The heat transfer coefficient is calculated as:

$$h = \frac{q''}{T_w - T_b} \tag{5.1.8}$$

where q'' is the heat flux, and T_w and T_b are the wall and fluid bulk temperatures, respectively. The Nusselt Number can be calculated as:

$$Nu = \frac{hD_h}{k} \tag{5.1.9}$$

Figure 5.1 shows variation of the temperature ratio $\left(\frac{T_{max} - T_b}{T_{max} - T_{in}}\right)$ with the Reynolds number for three locations of the absorbing plate in the channel and one solar concentration (C=1). Figure 5.2 shows variation of the temperature ratio with the Reynolds number for three locations of the absorbing plate in the channel and five solar concentrations (C=5). It should be noted that T_{max} represents the maximum temperature in the channel; T_b is the bulk temperature of the fluid and T_{in} is the inlet fluid temperature. The temperature ratio increases with increasing Reynolds number, which is more pronounced for $\mathrm{Re} \leq 150$. As the Reynolds number increases, the rise in the temperature ratio becomes gradual. High values of temperature ratio represent the low values of bulk temperature. It should be noted that the variation in the maximum temperature is small in the channel for all configurations of the absorbing plate. Consequently, increasing fluid bulk temperature lowers the temperature ratio. The convection heat transfer from the plate increases at high Reynolds number. This, in turn, lowers fluid bulk temperature, since mass flow rate increases at high Reynolds numbers. The location of the absorbing plate in the channel influences the temperature ratio significantly, which is more pronounced at high Reynolds numbers. In this case, the maximum temperature occurs at the surface of the absorbing plate and heat conduction and convection from the plate surfaces determines fluid bulk temperature. Consequently, location of the plate at the mid-height of the channel improves bulk temperature of the working fluid. Since the

absorption of the incident solar radiation is considered in the analysis, locating the absorbing plate at the bottom of the channel allows more radiation energy being absorbed by the fluid before reaching the absorbing plate. However, the amount absorbed energy by the fluid is considerably small, due to low absorption coefficient of the working fluid [42]. Therefore, fluid bulk temperature does not increase notably. Consequently the temperature ratio increases and becomes almost the same as that corresponding to the absorbing plate location at the top of the channel. Moreover, as the solar concentration increases (C = 5), temperature ratio reduces. This is attributed due to the followings;

i. The maximum temperature and the fluid bulk temperature increase in the flow and temperature difference between the maximum and the fluid bulk temperatures becomes small giving rise to low values of temperature ratio, and
ii. the maximum temperature increases with increasing solar concentration so that temperature difference between the maximum temperature and the fluid inlet temperature increases, which in turn lowers the temperature ratio. The location of absorbing plate at the top of the channel results in the highest temperature ratio then follows the locations at the bottom of the channel and at the mid-height of the channel. The attainment of high temperature ratio for the location of the absorbing plate at the top of the channel is attributed to the radiation losses from the plate's outer surface to its surroundings.

Figure 5.3 shows performance parameter (heat gain over heat input, Q_{gain}/Q_{in}) with the Reynolds number at different locations of absorbing plate in the channel and for one solar concentration (C=1). Figure 5.4 shows performance parameter with the Reynolds number at different locations of absorbing plate in the channel and five solar concentrations

(C=5). Increasing Reynolds number results in increased performance parameter. This is associated with the increased mass flow rate, which increases with increasing Reynolds number. Although temperature at the channel exit and bulk fluid temperature attain low values for high Reynolds numbers, increasing mass flow rate overcomes this shortcoming and enhances the performance parameter. In the case of different locations of the absorbing plate in the channel, the performance parameter increases considerably for the plate location at the center of the channel. This is attributed to the attainment of high bulk fluid temperature at the channel exit, which can also be observed from Figure 5.1 and Figure 5.2. However, the performance parameter becomes the lowest at the absorbing plate location of the top of the channel, which is true for all Reynolds numbers. As the solar concentration increases, so does the fluid bulk temperature at the channel exit. This gives rise to increased performance parameter as compared to solar concentration of one (C = 1). The influence of Reynolds number on the performance parameter for C = 5 is similar to that corresponding to C = 1. This is attributed to the mass flow rate, which increases with increasing Reynolds number. However, the location of the absorbing plate significantly influences the performance parameter; in which, the behavior of performance parameter differs for C = 5 than that of C = 1. The absorbing plate location at the top and center locations of the channel results in almost similar performance parameter behavior with increasing Reynolds number. This indicates that the gain of the solar energy absorbed by the fluid and by the absorbing plate located at the channel bottom is not significantly high.

Figure 5.5 shows the pump power loss parameter (pump power loss over heat gain, $\left(\frac{h_{p,L}}{Q_{gain}}\right)$ with Reynolds number for different locations of the absorbing plate in the channel and for one solar concentration (C=1). Figure 5.6 shows the pump power loss parameter with Reynolds number for different locations of the absorbing plate in the channel and for five solar concentrations (C=5). It should be noted that the pressure drop takes place along the channel length due to fluid friction, which is presented as $h_{p,L}$. The pump power loss parameter attains low values because of the small frictional loss along the channel and heat gain from the solar radiation is much higher than the pump power loss. The pump power loss parameter increases with increasing Reynolds number, which is more pronounced at high Reynolds numbers. The sudden increase in the pump power loss parameter at Re ≅ 180 is associated with the flow velocity, which increases with the Reynolds number. Since the increase in the frictional loss is not a linear function of the fluid velocity in the channel, the increase in the frictional loss appears to be sharp for Re>180. The absorbing plate locations at top and bottom of the channel results in almost similar pump power loss parameter. However, the absorbing plate location in the channel center gives rise to the highest pump power loss parameter. This is attributed to the boundary layer developed at the surface region of the plate; in which case, the rate of fluid strain remains high in this region. This, in turn, enhances the pressure drop in the channel; therefore, the pump power loss parameter increases considerably with increasing Reynolds number.

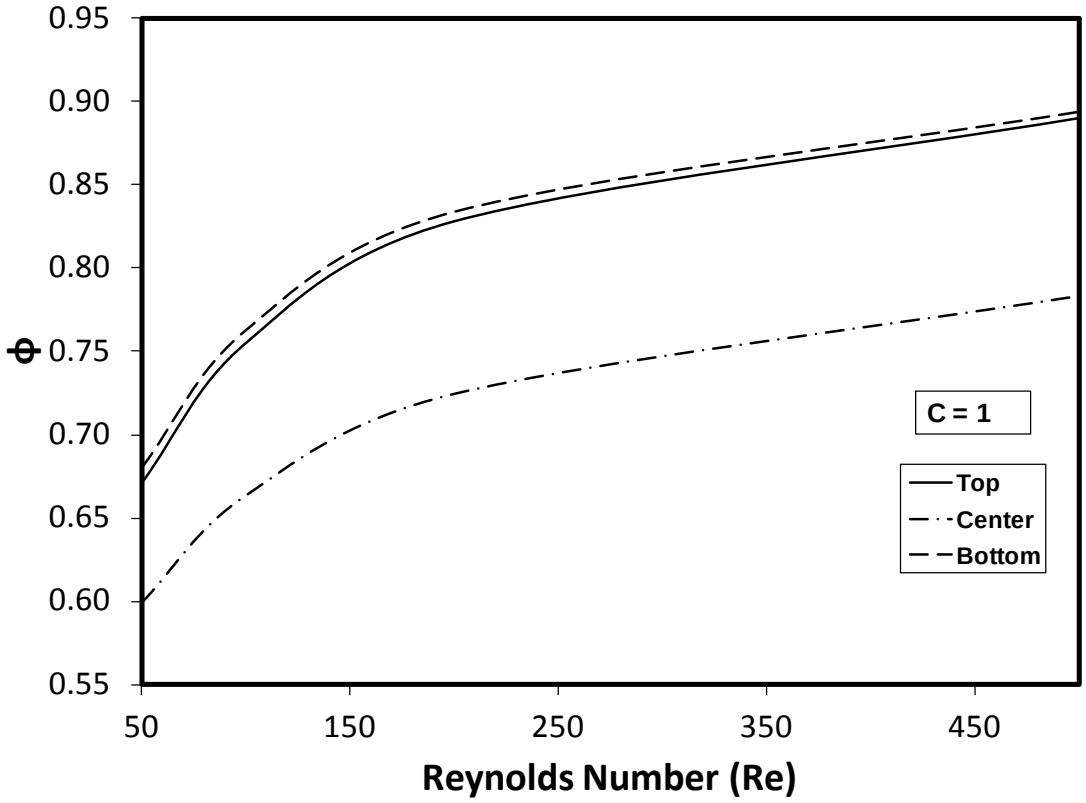

Figure 5.1. Temperature ratio ($\phi = \frac{T_{max} - T_b}{T_{max} - T_{in}}$) with Reynolds number

for concentration C = 1.

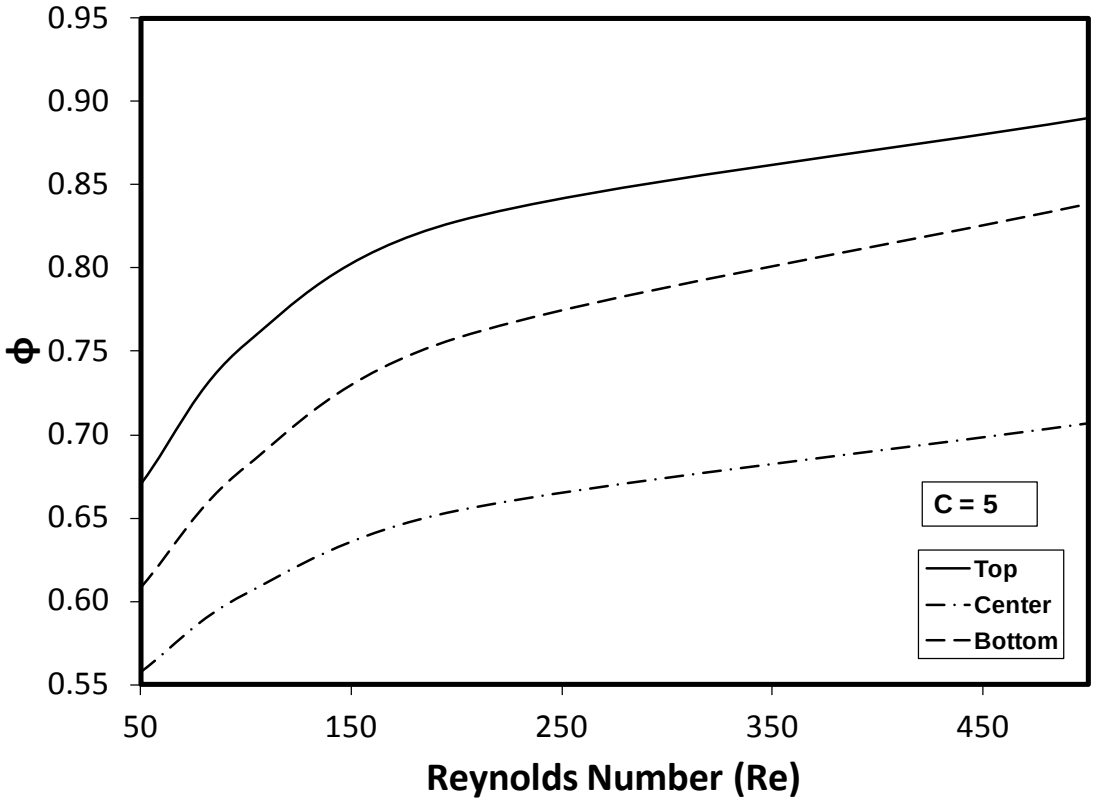

Figure 5.2. Temperature ratio ($\phi = \frac{T_{max} - T_b}{T_{max} - T_{in}}$) with Reynolds number

for concentration C = 5.

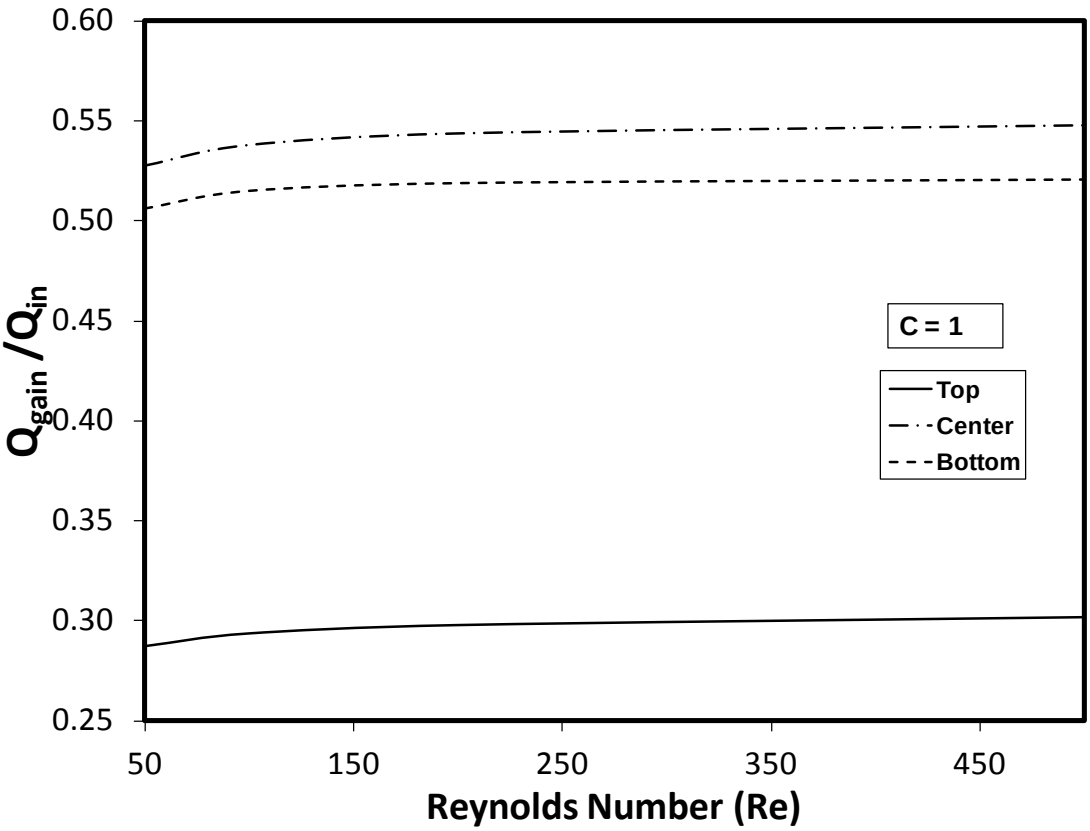

Figure 5.3. Performance parameter (Q_{gain}/Q_{in}) with Reynolds number

for concentration C = 1.

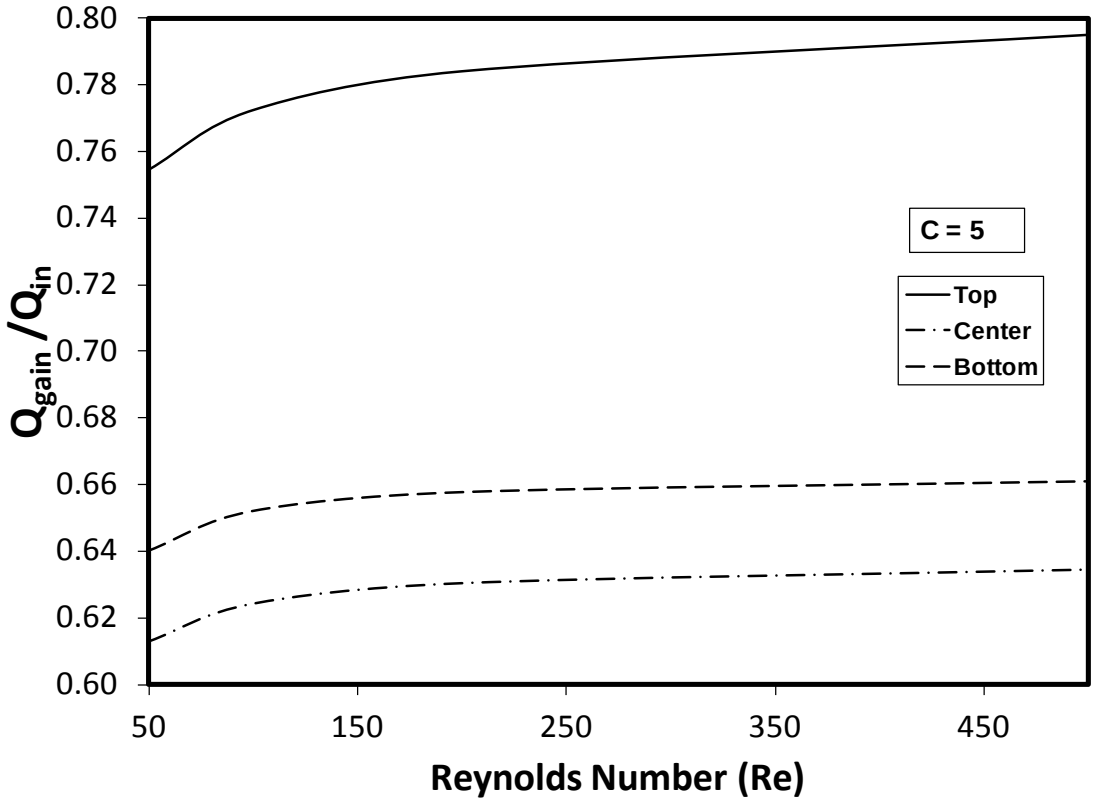

Figure 5.4. Performance parameter (Q_{gain}/Q_{in}) with Reynolds number

for concentration C = 5.

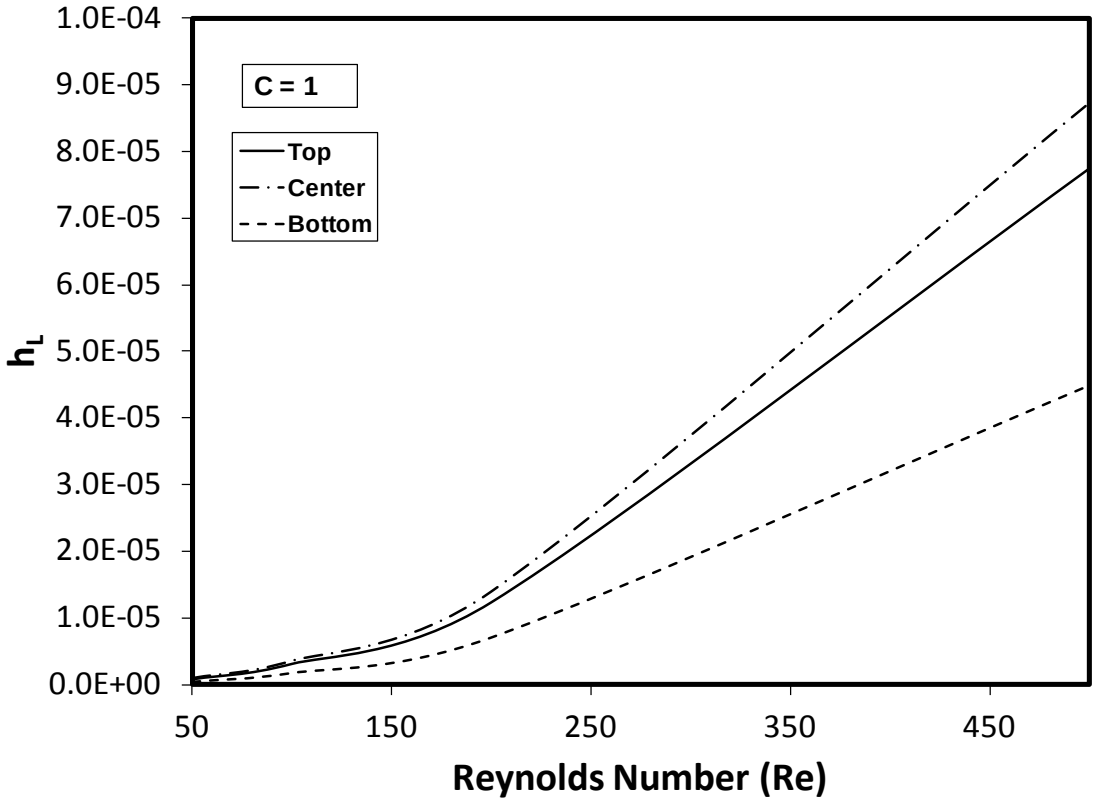

Figure 5.5. Pump power loss parameter ($\frac{h_{p,L}}{Q_{gain}}$) with Reynolds number

for concentration C = 1.

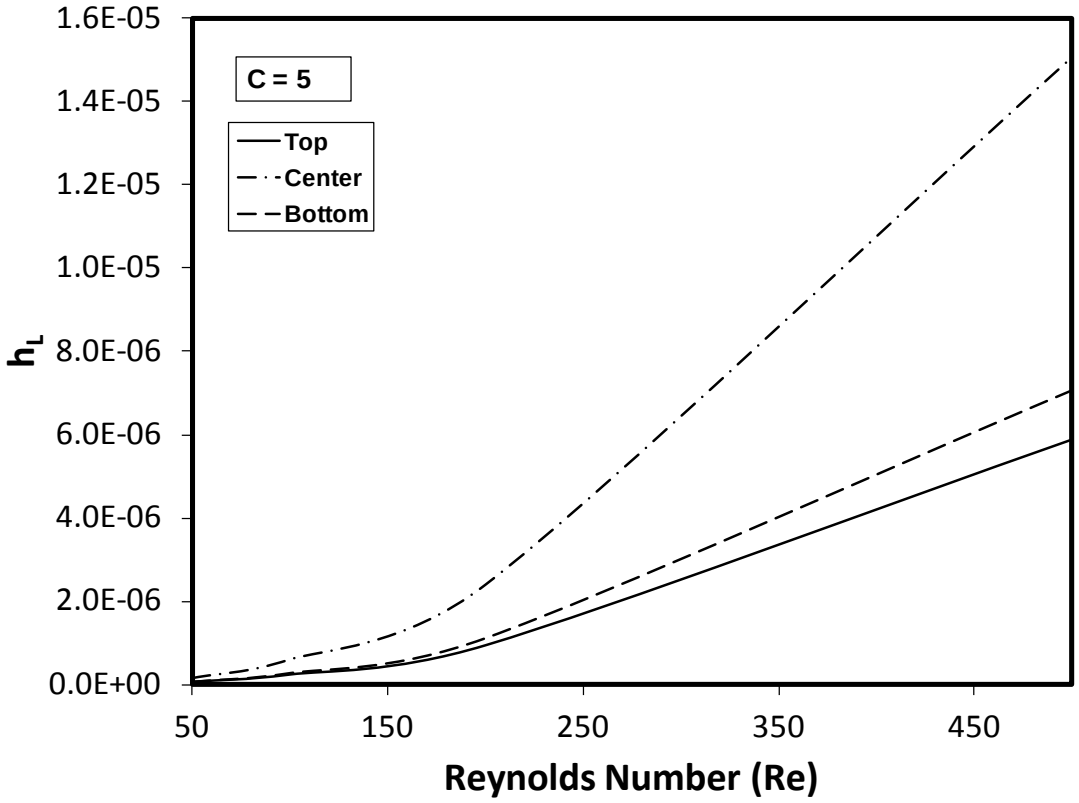

Figure 5.6. Pump power loss parameter ($\frac{h_{p,L}}{Q_{gain}}$) with Reynolds number

for concentration C = 5.

5.2 Low Reynolds Number with P.C.M.

The performance of the volumetric solar absorption system, including the absorbing plate and the phase change particles (P.C.M.) in the channel flow, is investigated for various lower Reynolds numbers.

Figure 5.7 shows the Nusselt number variation along the solar absorber plate for various Reynolds numbers. The location of the absorber plate is at the top surface of the channel. The Nusselt number increases in the neighborhood of the absorber plate inlet. The increase in the Nusselt number is associated with the phase change particles. In this case, temperature rise in the fluid is suppressed by the phase change particles in the vicinity of the absorber plate wall. This, in turn, results in increased temperature difference between the fluid and the absorber plate wall while enhancing the Nusselt number. However, once the phase change is completed, the fluid temperature increases due to the sensible heating of the fluid. The Nusselt number, then, reduces accordingly. The similar behavior of the Nusslet number is also observed in the previous study [36]. Once the phase change particles are completely dissolved in the carrier fluid, temperature difference between the fluid and the absorber wall remains almost the same along the channel length. This results in constant Nusselt number along the remaining section of the channel length. Increasing Reynolds number shifts the location of the initiation of the phase change along the absorber surface. This is because of the forced convection effect; in which case, the fluid temperature remains low in the initial segment of the absorber wall. Therefore, the fluid temperature reaching the liquidus temperature of the phase change particles is delayed along the absorber wall. Once the phase change initiates, the Nusselt number

increases and its behavior becomes almost similar to that corresponding to the low Reynolds numbers. Although the sensible heating of the fluid enhances after completion of the phase change at high Reynolds numbers, the Nusselt number variation does not alter notably in the downstream of the channel length. It should be noted that the fluid bulk temperature reduces slightly with increasing Reynolds number after the completion of the phase change in the fluid. The Nusselt number variation is also shown in (Figure 5.8), (Figure 5.9) and (Figure 5.10) for the absorber plate locations of at the mid-height and at the bottom of the channel as well as at the bottom of the channel only, respectively. It should be noted that the Nusselt number variation is presented along the absorber wall. Since two surfaces of absorber are present, Nusselt number variations are presented for two surfaces of the absorber at location of the mid-height of the channel. The Nusselt number variation shows similar behavior for all locations to that corresponding to the top surface, provided that the Nusselt number increases slightly at the bottom surface of the absorber, which is located at the mid-height of the channel. The Nusselt number enhancement is attributed to the low fluid temperature between the absorber and the bottom wall of the channel. Although the radiation absorption by the fluid in the channel is incorporated in the simulations, the absorber plate is considered to transmit only 50% of the incident solar radiation towards the bottom wall of the channel. Therefore, the absorber wall temperature becomes higher than the bulk fluid temperature between the absorber and the bottom wall. This, in turn, enhances the heat transfer rates from the absorber bottom wall to the neighboring fluid while enhancing the Nusselt number along the absorber bottom wall. In the case of absorber location at the bottom

wall (Figure 5.10), the peak Nusselt number increases with increasing Reynolds number. This behavior is attributed to the low fluid temperature near the absorber wall region due to high convection current. Although high Reynolds number delays the phase change in the absorber wall vicinity, it improves the peak value of the Nusselt number in the channel. The similar behavior is also observed for the absorber location at the mid-height of the channel. The Nusselt number behavior at the top and bottom surfaces of the plate differs slightly from each other. In this case, a sharp decay of the Nusselt number is observed from its peak value, which indicates the attainment of slightly high fluid temperature towards the downstream along the absorber wall.

Figure 5.11 show contour plots of temperature and the specific heat in the channel for different locations of the absorber plate and for the Reynolds number Re = 7. Temperature of the fluid increases towards the downstream of the channel, particularly in the region of the absorber plate. This is case convection, conduction, and radiation heat transfer from the absorber plate as well as the incident solar radiation by the fluid are responsible fluid temperature increase in the flow downstream.

Figure 5.12 show contour plots of temperature and the specific heat in the channel for different locations of the absorber plate and for the Reynolds number Re = 7. The increase in the specific heat is associated with the phase change of the P.C.M. particles in the channel. It is evident that the phase change completes almost at the initial length of the absorber plate where the Nusselt number is high. Once the phase change is completed, the fluid bulk temperature increases due to the sensible heating. This, in turn,

suppresses the Nusselt number increase in the absorber wall vicinity in the downstream of the absorber plate.

Figure 5.13 shows the performance parameter (Q_{gain}/Q_{in}) with the Reynolds number for the absorber plate location at the top surface of the channel. The performance parameter for water is also shown for the comparison. The performance parameter increases with increasing Reynolds number. This is associated with the energy gain due to increased mass flow rate at high Reynolds number, despite the fact that the fluid bulk temperature reduces with increasing Reynolds number. The performance parameter is higher for the carrier fluid with P.C.M. particles as compared to water alone. This is because of the energy gain of the working fluid due to the latent heat of melting of the P.C.M. particles. However, the thermal energy gain as compared to water alone is slightly higher at low Reynolds number than that corresponding to the high Reynolds number. This indicates that the completion of the phase change in the early stage, due to low Reynolds number flow, enables the working fluid to gain thermal energy through sensible heating. In this case, early completion of the phase change results in high fluid bulk temperature towards the exit of the channel. However, the magnitude of the performance parameter becomes less for the absorber plate location at the mid-height of the channel. Therefore, locating the absorber plate at the channel mid-height does not gives rise to better thermal performance in terms of thermal energy gain by the fluid as compared to corresponding to the absorber location at the top surface. The radiation loss from the channel top surface is incorporated in the simulations for both absorber plate locations. Although, temperature of the plate attains high values for the location at the surface, the emissivity

of the absorber plate is low ($\varepsilon = 0.039$). It should be noted that the absorber plate is considered to have the selective surface coated by ZrN. Therefore, the radiation losses from the surface become small. The performance parameter for the absorber plate location at the bottom of the channel is larger than the other locations of the absorber plate in the channel. In this case, absorption of incident solar radiation by the fluid as well as by the selective surface at the channel bottom contributes to the increase in the fluid bulk temperature. It should be noted that the radiation model, which is incorporated in the simulations, allows the absorption of incident radiation by the fluid. Moreover, the performance parameter also attains higher values for water where the absorber plate location is at the bottom of the channel as compared to those corresponding to the other locations. This is associated with the convective heating of the absorbing plate and the energy gain by the fluid through absorption of the incident solar radiation.

Figure 5.14 shows pump power loss parameter for different absorber plate locations in the channel. The presence of P.C.M. particles enhances the pump power loss parameter, which is more pronounced at high Reynolds numbers, the viscosity of the carrier fluid increases with the presence of P.C.M. particles in the carrier fluid. This, in turn, increases the frictional drag in the channel. In the case of absorber plate location at the channel bottom, the behavior of the pump power loss parameter is similar to that corresponding to the absorber plate at the top surface of the channel. However, this behavior differs significantly for the absorber plate location at the mid-height of the channel as compared to the other locations of the absorber plate. This is associated with the frictional drag developed at the top and bottom surfaces of the absorber plate as well as the pressure

drag formed due to the thickness of the absorber plate. In this case, the value of the pump power loss parameter increases almost double of that corresponding to the other locations of the absorber plate.

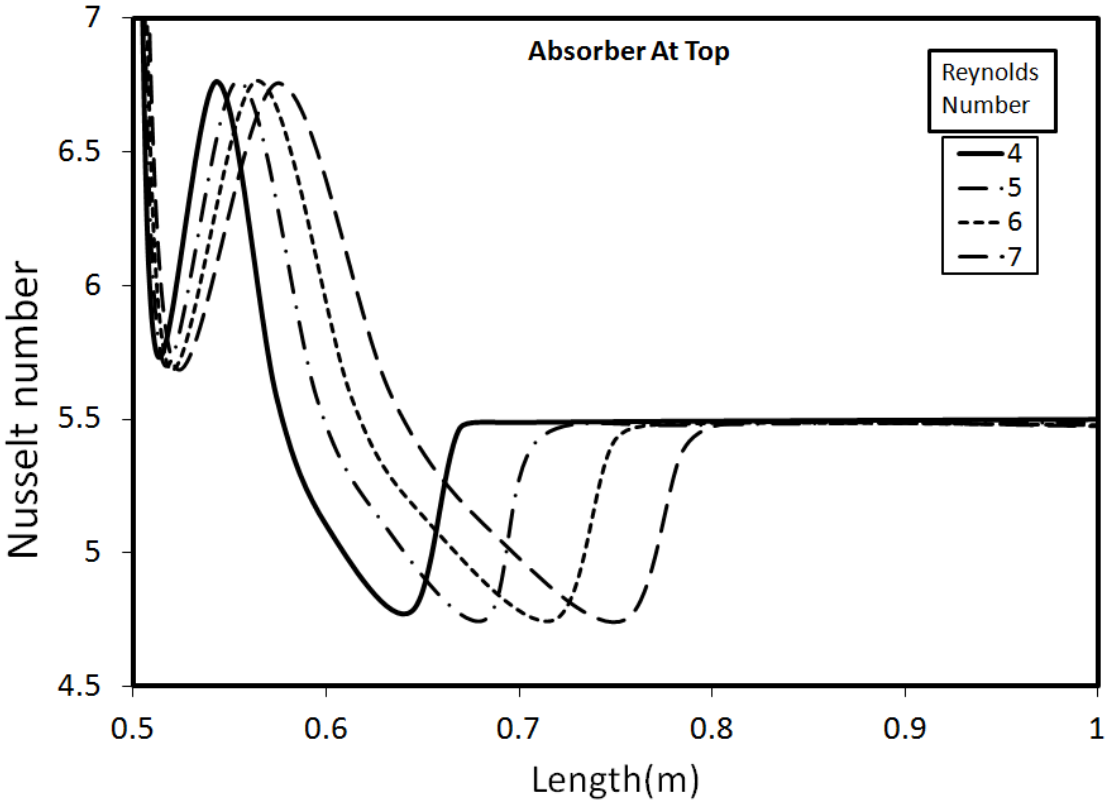

Figure 5.7. Nusselt number variation along the absorber plate surface in the channel for various Nusselt numbers. The absorber location is at the top of the channel.

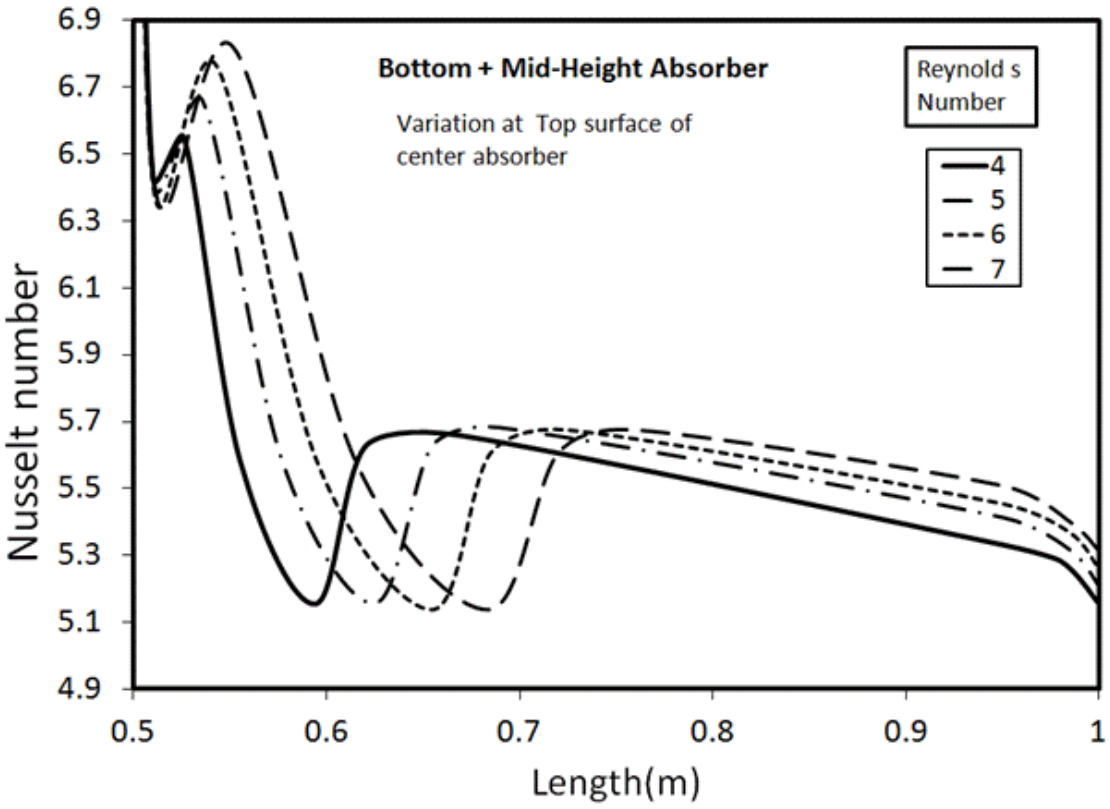

Figure 5.8. Nusselt number variation along the absorber plate surfaces in the channel for various Nusselt numbers. The absorber location is at the mid-height and at the bottom of the channel. The Variation is for top surface of the center absorber.

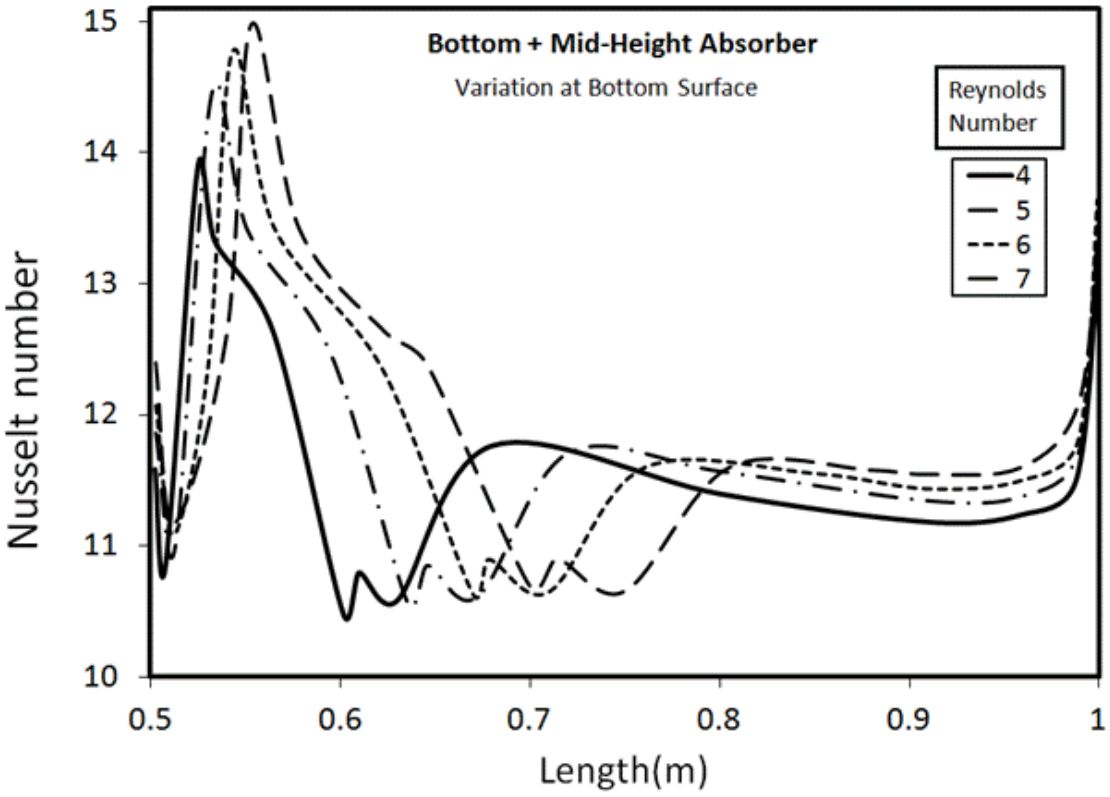

Figure 5.9. Nusselt number variation along the absorber plate surfaces in the channel for various Nusselt numbers. The absorber location is at the mid-height and at the bottom of the channel. The variation is for bottom surface of the absorber.

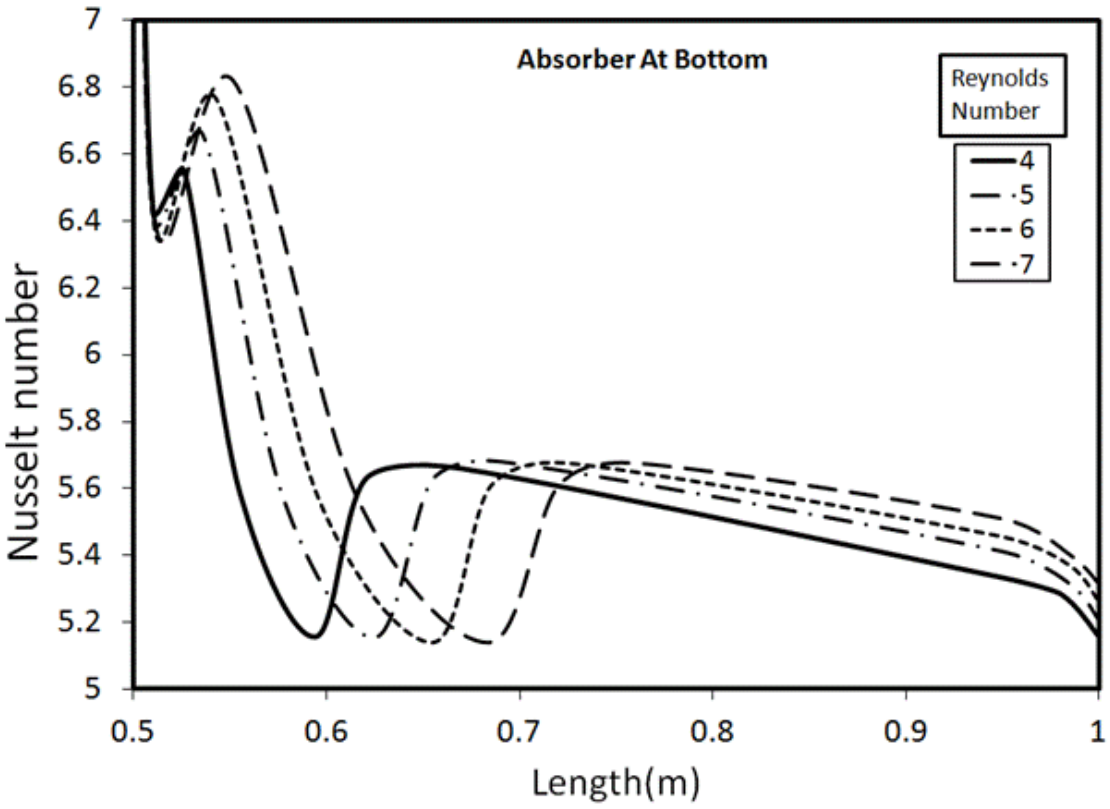

Figure 5.10. Nusselt number variation along the absorber surfaces in the channel for various Nusselt numbers. The absorber plate location is at the bottom of the channel only.

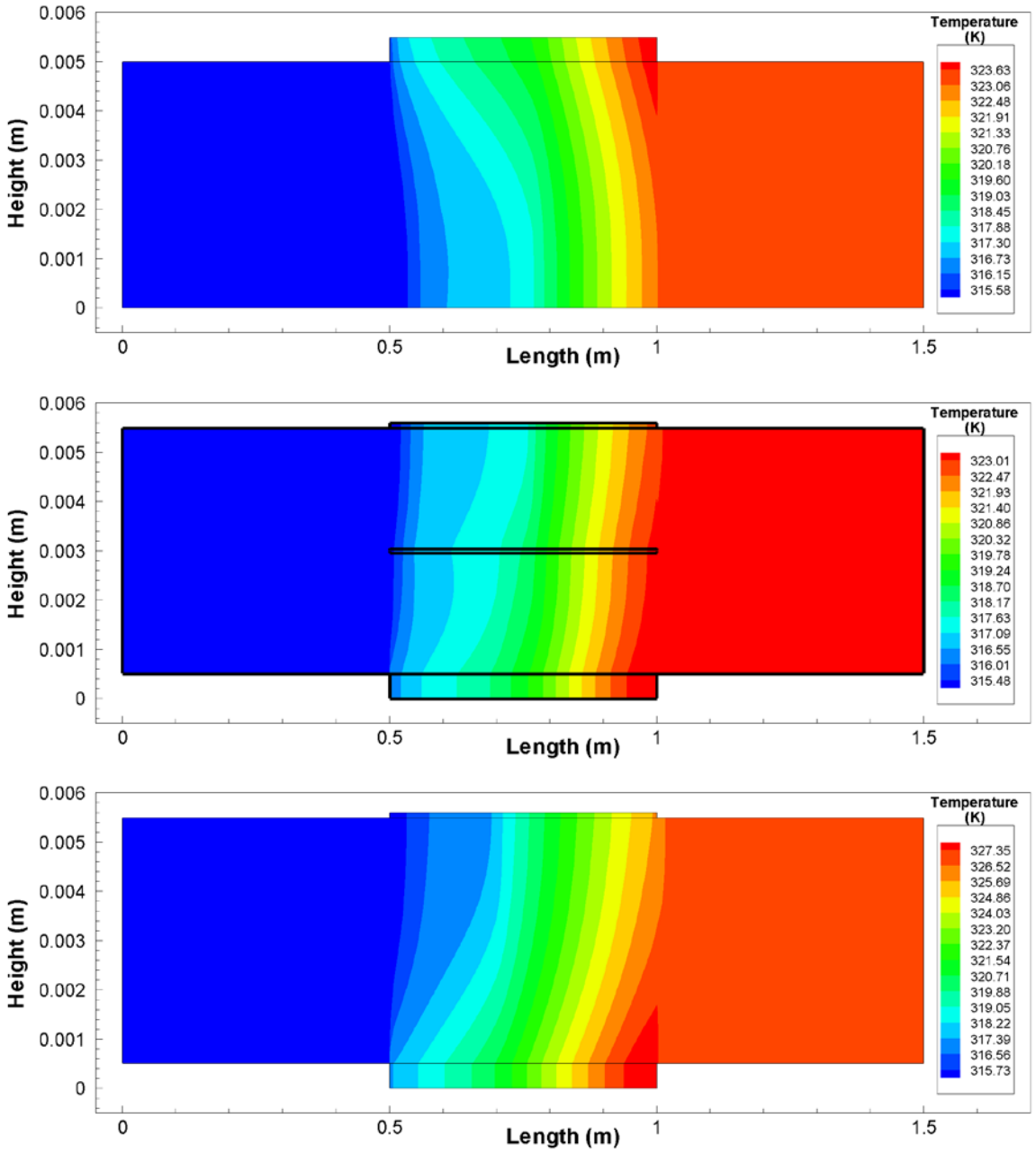

Figure 5.11. Temperature contours in the channel for different locations of absorbing plate. The carrier fluid contains 7% (by volume) of P.C.M. particles and the Reynolds number is 7.

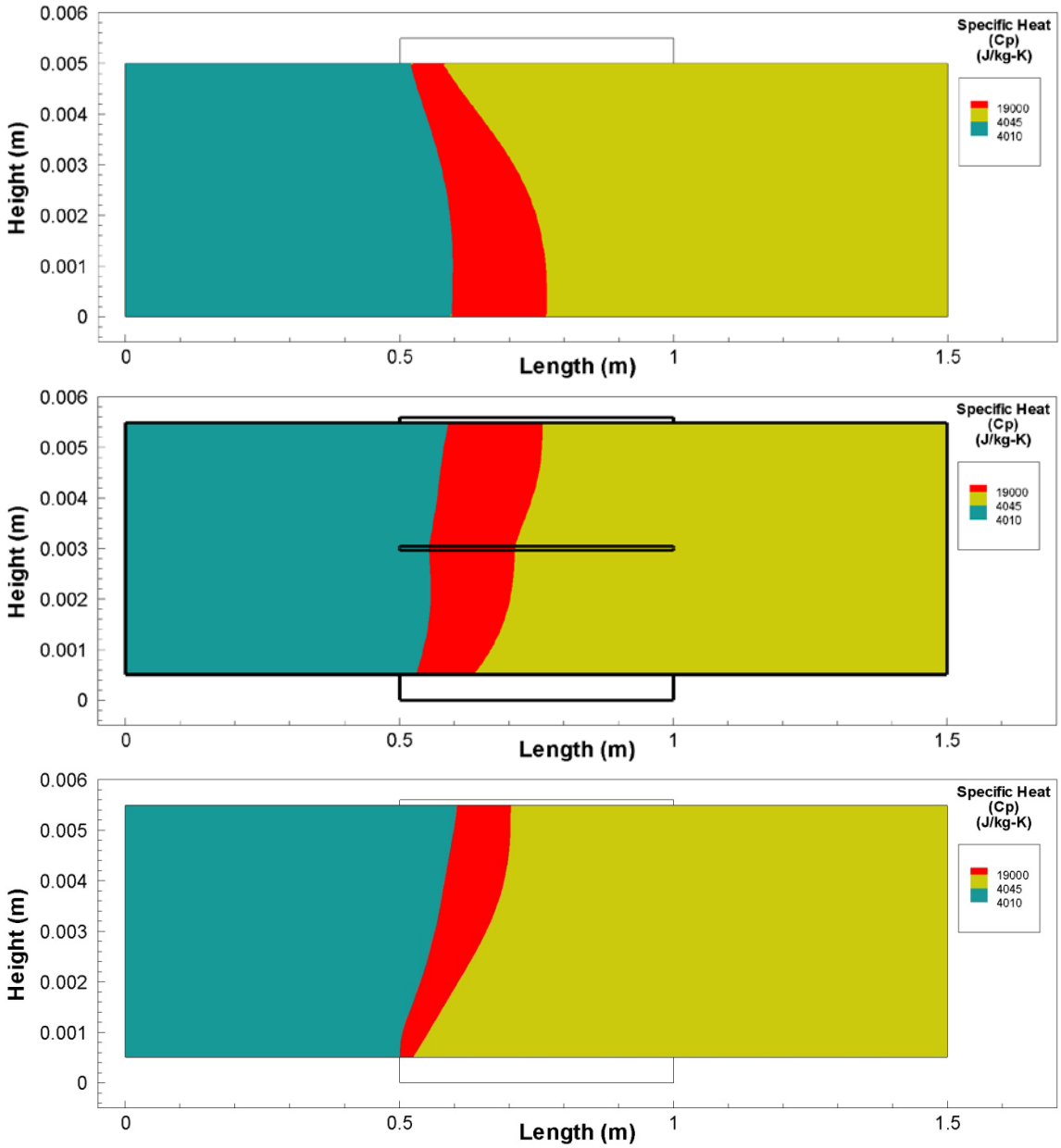

Figure 5.12. Contours of specific heat in the channel for different locations of absorbing plate. The carrier fluid contains 7% (by volume) of P.C.M. particles and the Reynolds number is 7.

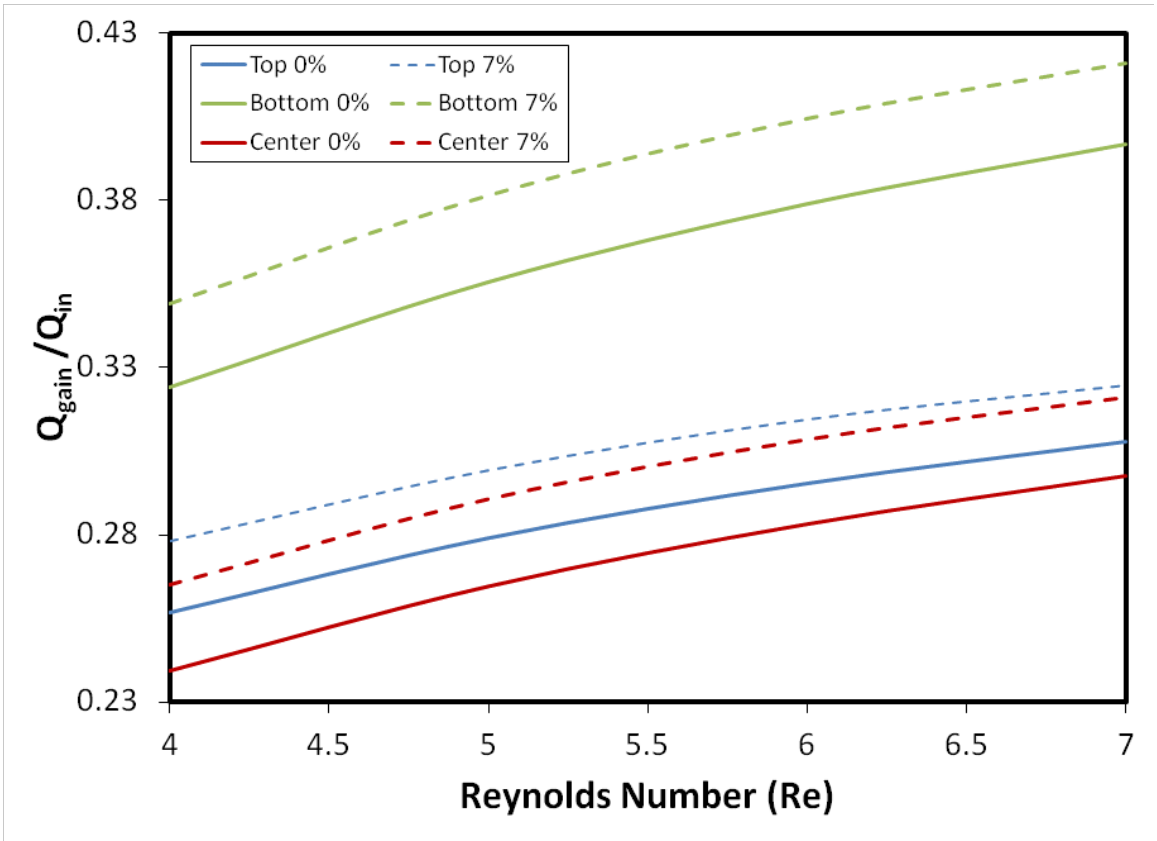

Figure 5.13. Performance parameter with Reynolds number for the carrier fluid with (0%) no P.C.M. particles and with 7% (by volume) P.C.M. particles and for three different absorber locations in the channel.

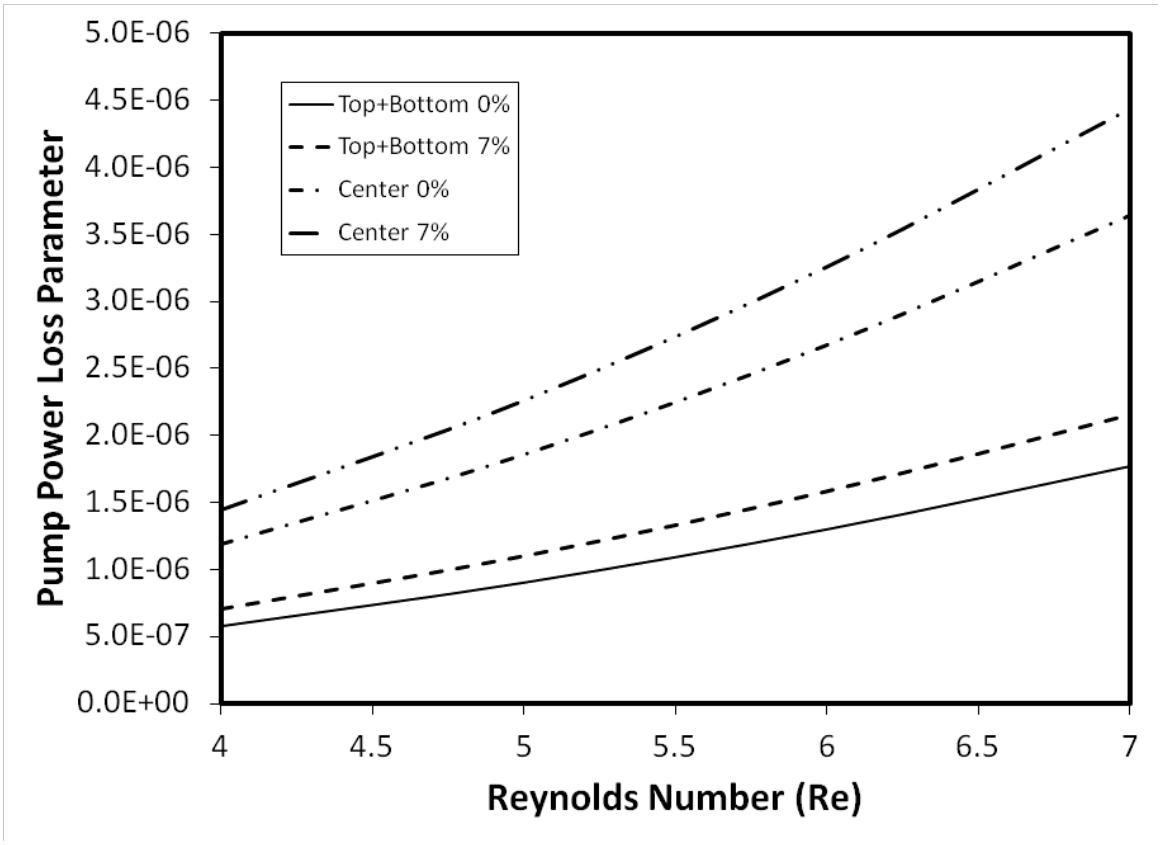

Figure 5.14. Pump power loss parameter with Reynolds number for the carrier fluid with no P.C.M. particles and with 7% (by volume) P.C.M. particles and different absorber plate locations in the channel. Since the pump power loss parameter due to water (0% P.C.M. particles) is identical for the absorber plate locations at the top and at the bottom of the channel, curve legend of Top+Bottom is used for this purpose.

5.3 High Reynolds Number with P.C.M.

The performance characteristics of solar volumetric absorption system consisting of absorber plate and channel flow with presence of phase change particles are investigated for various solar concentrations and high flow Reynolds numbers. The absorber plate is placed in three different locations in the channel to assess the influence of absorber plate location on the heat transfer rates in the channel.

Figure 5.17, Figure 5.16 and Figure 5.17 shows temperature contours in the channel at different locations of the absorber plate for solar concentration C = 5 and two Reynolds numbers (Re = 50 and Re = 100). The influence of the absorber plate location on temperature filed is clearly observed from the figures. In addition, changing Reynolds number effects the temperature distribution in the channel. This is associated with the distribution of amount of solar absorption in the channel; in which case, changing the location of the absorber plate alters the energy absorbed from the solar radiation in the channel. The phase change of P.C.M. particles takes place once the melting temperature is reached. This suppresses the temperature rise locally in the channel until the phase change completes. Sensible heating takes over immediately after the melting is completed above the liquidus temperature of phase change particles; this, in turn, enhances temperature increase in the channel.

Figure 5.18 and Figure 5.19 show the Nusselt number variation along the absorber plate for different solar concentrations and two Reynolds numbers, respectively. It should be

noted that the absorber plate location is at the top surface of the channel (Figure 3.5). The Nusselt number reduces along the length of the absorber plate, which is more pronounced for high solar concentration. Although the concentration of the phase change particle is 7%, phase change particles melts almost instantly because of the attainment of high fluid temperature in the vicinity of the absorber surface. It should be noted that introducing high solar concentration at the absorber surface enhances temperature of absorber plate and fluid in the neighborhood of the absorber plate surface. This, in turn, lowers temperature difference between absorber and working fluid; thereby, lowering the Nusselt number along the absorber plate surface. As the solar concentration reduces (C = 5), difference between the absorber plate wall temperature and temperature of working fluid in its neighborhood becomes less, which in turn gives rise to slight changes in Nusselt number. The Nusselt number reduces slightly in the close region of the absorber plate length of 0.8 m. This occurs for solar concentration C = 5, which is attributed to the end of phase change of P.C.M. particles where fluid temperature increases to the liquidus temperature of P.C.M. particles; in which case, sensible heating enhances the fluid temperature while lowering temperature difference between the absorber plate wall and its neighborhood fluid temperatures. Consequently, the Nusselt number attains slightly low values in this region. When comparing Figure 5.18 and Figure 5.19, it can be observed that the behavior of the Nusselt number is almost the same for both Reynolds numbers, despite the fact that increasing Reynolds number increase the fluid inertia force; thereby, thinning the thermal boundary layer in the vicinity of the absorber plate wall.

Figure 5.20 and Figure 5.21 show the Nusselt number variation along the absorber plate surface for different solar concentrations and two Reynolds numbers, respectively. It should be noted that the absorber plate is located at the bottom of the channel. In the simulations, radiation model incorporates absorption, emission, and transmittance of the incident solar radiation within the working fluid. Therefore, incident solar radiation undergoes partially absorption and scattering by the working fluid prior reaching to the absorber plate at the channel bottom. The Nusselt number reduces along absorbing plate length. However, the Nusselt number attains slightly higher values for low solar concentration. In this case, complete melting of phase change particles takes place in the downstream region of the absorber plate. Therefore, fluid temperature in the neighborhood of the absorber plate remains within the range of solidus and liquidus temperatures of the phase change particles. This, in turn, enhances the Nusselt number slightly for low solar concentration. The effect of Reynolds number on the Nusselt number variation becomes visible along the absorber plate length $0.6 \leq \text{Length} \leq 0.9$. In this case, contribution of the phase change particles to maintain low fluid bulk temperature changes while modifying the Nusselt number along the absorber plate surface. However, this effect is not significantly high, since Nusselt number variation is on the order of few percent only.

Figure 5.22 and Figure 5.23 show the Nusselt number variation along the absorber plate surface located at the channel bottom for different solar concentrations and two Reynolds numbers, respectively. However, additional solar absorber is located at the mid-height of the channel and solar absorber is considered to have 50% transmittance capacity to the

incident solar radiation. Therefore, absorber plate located at the channel bottom enables to absorb the transmitted solar radiation through the first solar absorber at the channel mid-height. Although the radiation model incorporates absorption of incident solar radiation by the working fluid, significant amount of absorption takes place by the solar absorber at the channel mid-height and absorber plate at the channel bottom. However, consideration of 50% transmittance of the absorber plate at the channel mid-height lowers the absorber plate temperature at the channel bottom. Consequently, heat transfer from the absorber plate to the working fluid causes gradual progressing of the phase change along the absorber plate surface at the channel bottom. Since the liquidus and solidus temperature difference is 1°C, the phase change of the particles suppresses the working fluid temperature increase in the vicinity of the absorber plate. Therefore, the Nusselt number increases significantly along the absorber plate surface. In addition, lowering solar concentration extends the phase change process towards the downstream of the absorber plate while delaying the completion of the phase change in this region. This situation is also seen at high Reynolds number (Re=100). Although the behavior of the Nusselt number along the plate surface for two Reynolds number is similar, the length scale where the phase change is completed influences the magnitude of the Nusselt number at the channel bottom. When comparing the Nusselt number for different locations of the absorber plate (Figure 5.18, Figure 5.20, Figure 5.22) for all Reynolds numbers considered in the current study, it is evident that the absorber plate location at the mid-channel height results in the highest Nusselt number.

Figure 5.24, Figure 5.25 and Figure 5.26 show the performance parameter (Q_{gain}/Q_{in}) with the Reynolds number at different locations of absorber plate for different solar concentrations. It is evident that increasing solar concentration enhances the performance parameter, provided that the location of absorber plate influences this variation with the Reynolds number. In this case, the performance parameter increases almost linearly with increasing Reynolds number. As the absorber plate location changes to mid-height of the channel and to the channel bottom, the performance parameter reduces almost linearly with increasing Reynolds number for low solar concentration (C = 5). This indicates that operating solar volumetric absorber system incorporating the absorber plate at the mid-height of the channel lowers the thermal performance of the system at high Reynolds number. Increasing performance parameter with increasing Reynolds number is associated with the increased mass flow rate at high Reynolds numbers. Since, Q_{gain} (heat gain) increases with increased mass flow rate while Q_{in} remains the same for given solar concentration. When comparing the performance parameter at different locations of the absorber plate in the channel, one can observe that the absorber plate at the top of the channel results in the highest performance parameter. Consequently, using the selective surface with low reflectivity and emissivity at the top of the channel gives rise to the highest performance parameter for the range of solar concentrations and volume fractions of phase change particles used in the system. In addition, operating the system at high solar concentration is fruitful, since the performance parameter improves notably.

Figure 5.27 shows pump power loss parameter, as defined in equation(5.1.5), with Reynolds number at different locations of the absorber plate in the channel. The pump

power loss is associated with the frictional loss in the channel and pressure drop due to the presence of the absorber plate at the mid-height of the channel. The pump power loss parameter increases with increasing Reynolds number. Since the fluid friction in the channel increases with increasing Reynolds number, the pump power loss parameter also increases at high Reynolds numbers. Since the absorber plate surface is leveled with the channel wall when its locations are at the top and the bottom of the channel, the pump power loss parameter becomes identical at these locations of the absorber plate. The pump power loss parameter increases significantly for the absorber plate location at the mid-height of the channel. This is attributed to:

i. pressure loss due to pressure drag, and
ii. enhancement of the frictional loss due to exposure of both surface of the absorber plate to the working fluid. Consequently, absorber plate location at the mid-height of the channel increases significantly the hydrodynamic losses in the channel.

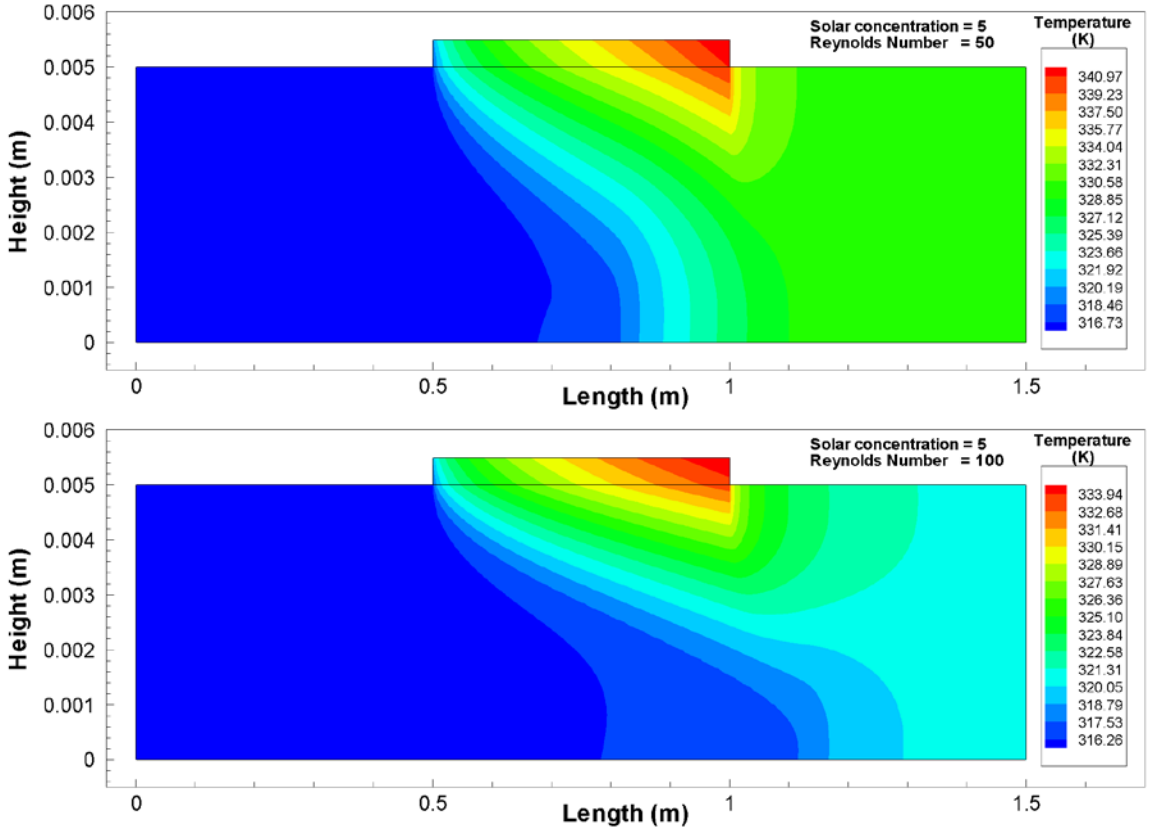

Figure 5.15. Temperature contours in the channel for Top absorber plate location.

C = 5 , Re = 20, 100

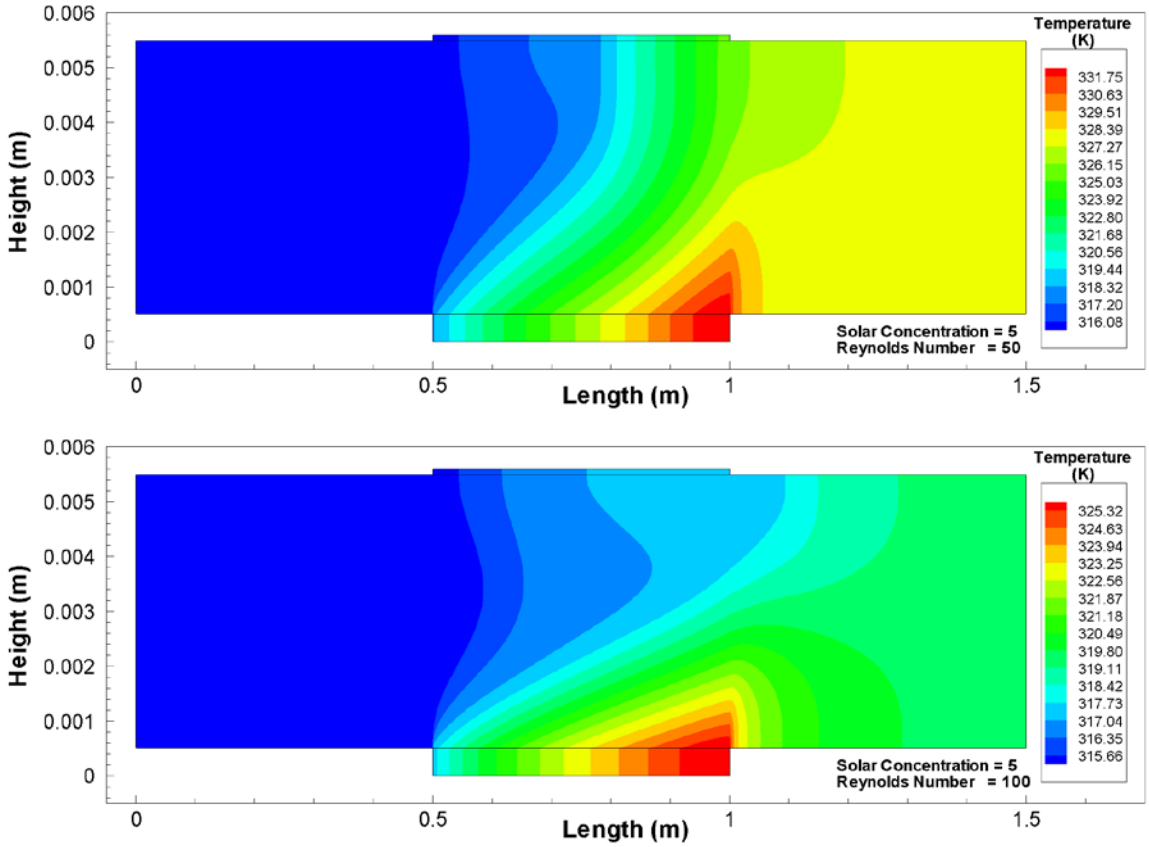

Figure 5.16. Temperature contours in the channel for different absorber plate locations.

C = 5 Re = 20, 100

.

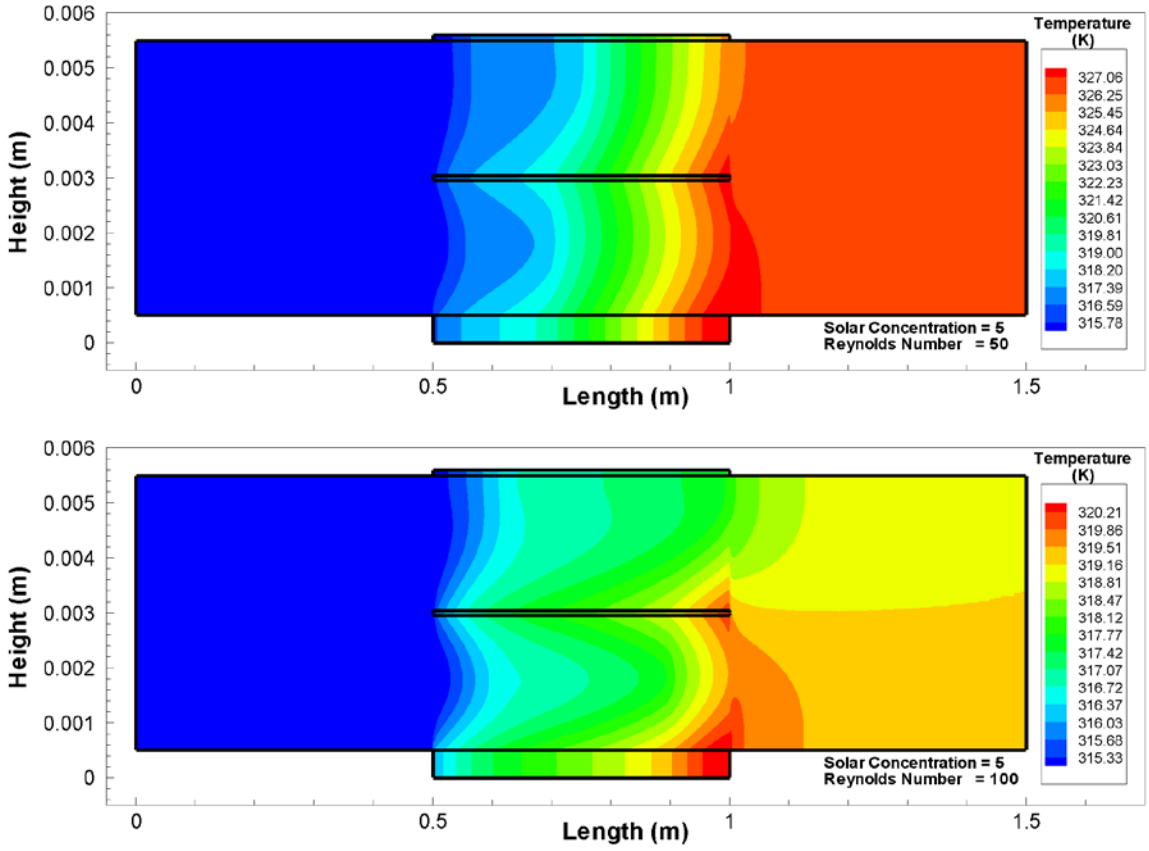

Figure 5.17. Temperature contours in the channel for different absorber plate locations.

C = 5 Re = 20, 100

.

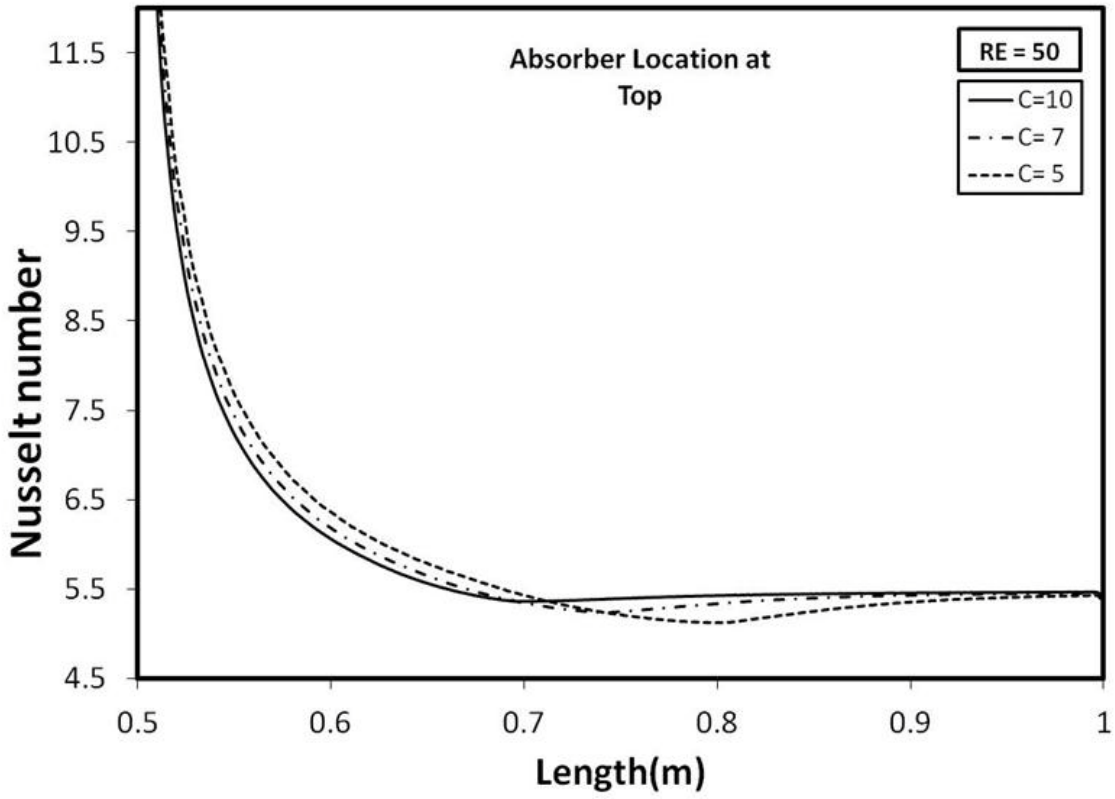

Figure 5.18. Nusselt number variation along the absorber plate for different concentrations and Re = 50. The absorber plate is at the top of the channel.

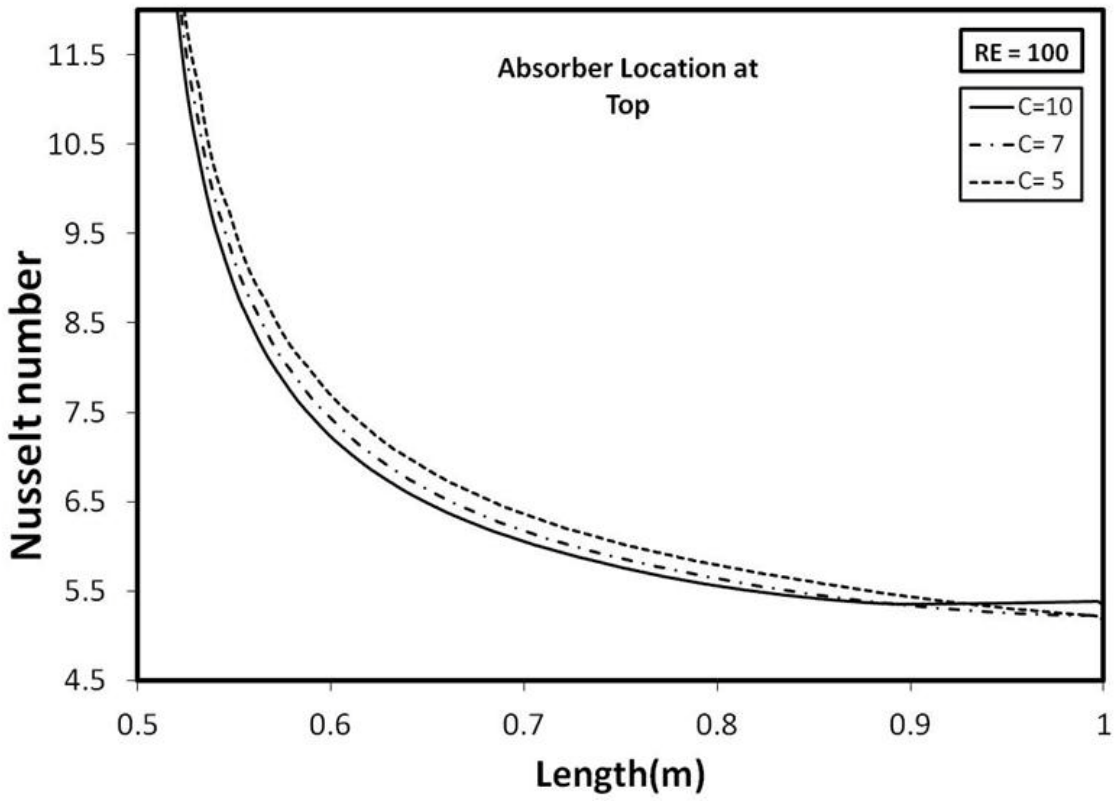

Figure 5.19. Nusselt number variation along the absorber plate for different concentrations and Re = 100. The absorber plate is at the top of the channel.

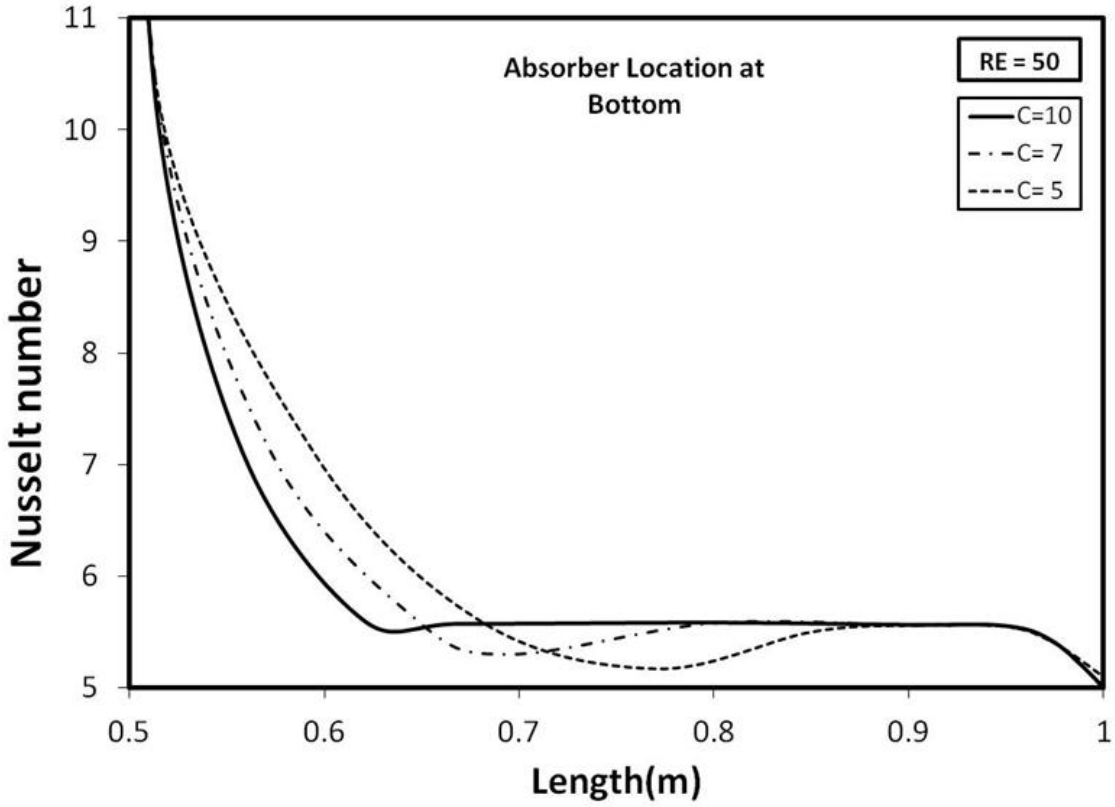

Figure 5.20. Nusselt number variation along the absorber plate for different concentrations and Re = 50. The absorber plate is at the bottom of the channel.

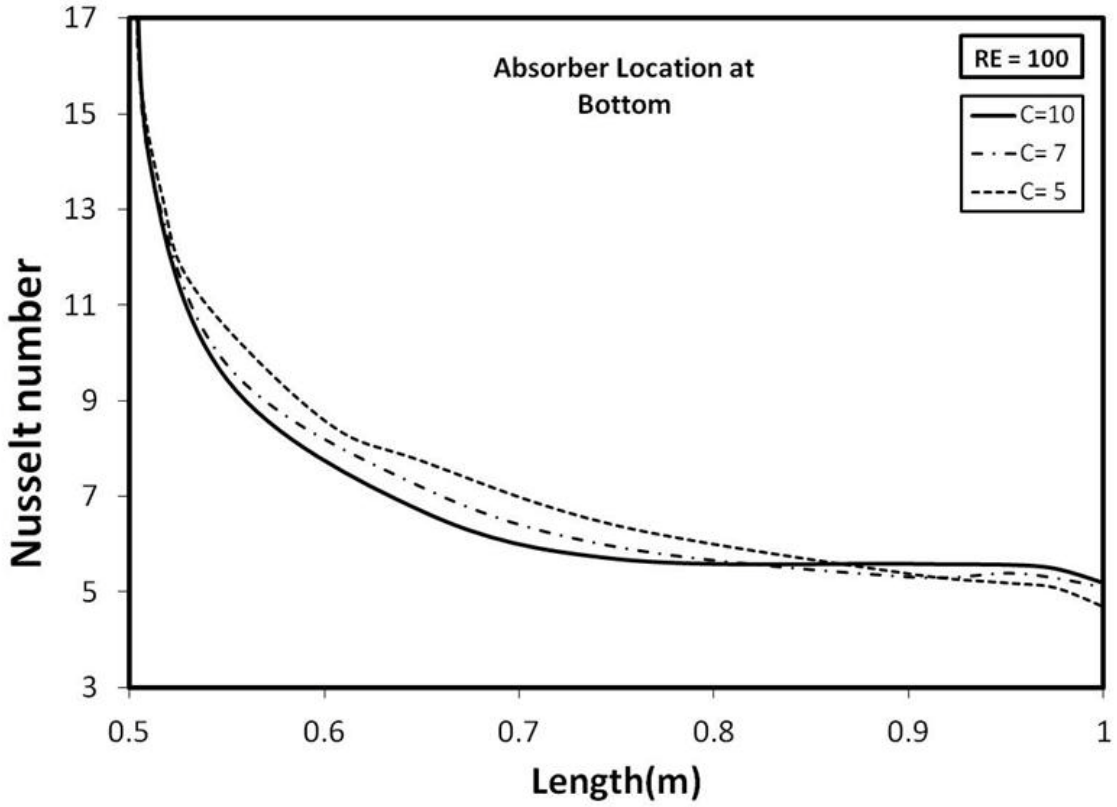

Figure 5.21. Nusselt number variation along the absorber plate for different concentrations and Re = 100. The absorber plate is at the bottom of the channel.

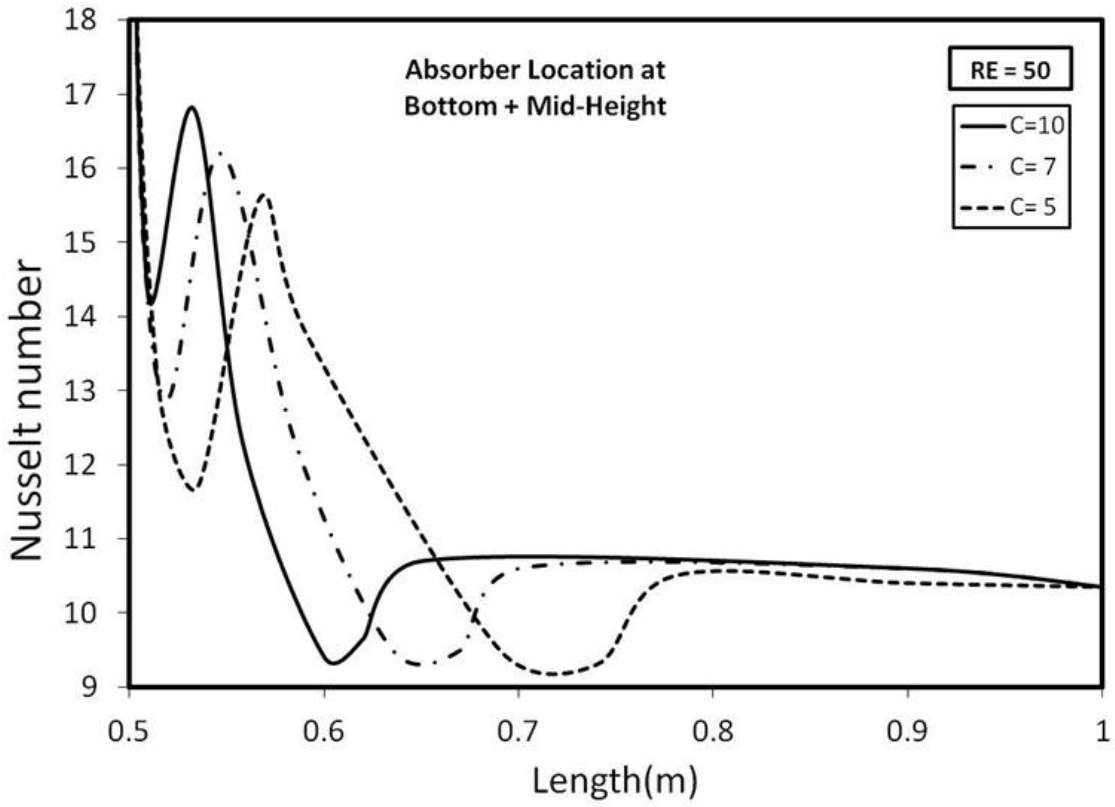

Figure 5.22. Nusselt number variation along the absorber plate for different concentrations and Re = 50. The absorber plate is at the bottom of the channel and 50% transmitted absorber at the mid-height of the channel. Variation at Top Surface of Center Absorber

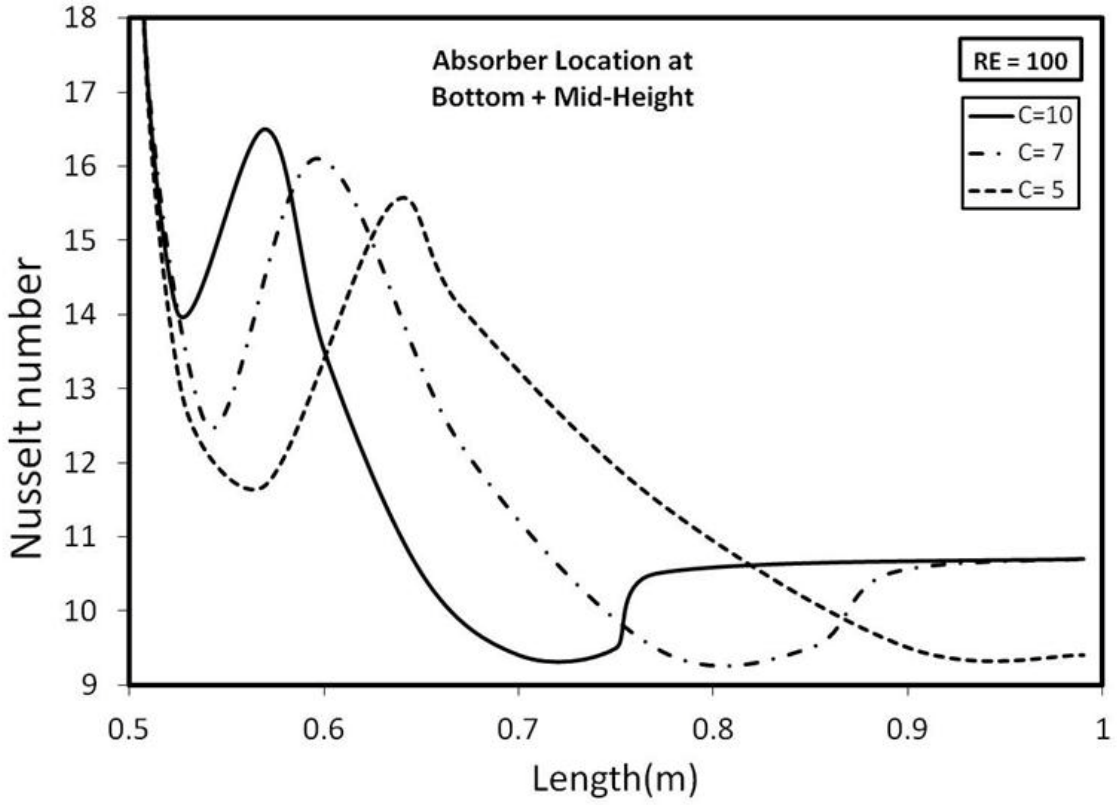

Figure 5.23. Nusselt number variation along the absorber plate for different concentrations and Re = 100. The absorber plate is at the bottom of the channel and 50% transmitted absorber at the mid-height of the channel. Variation at Bottom Surface is shown.

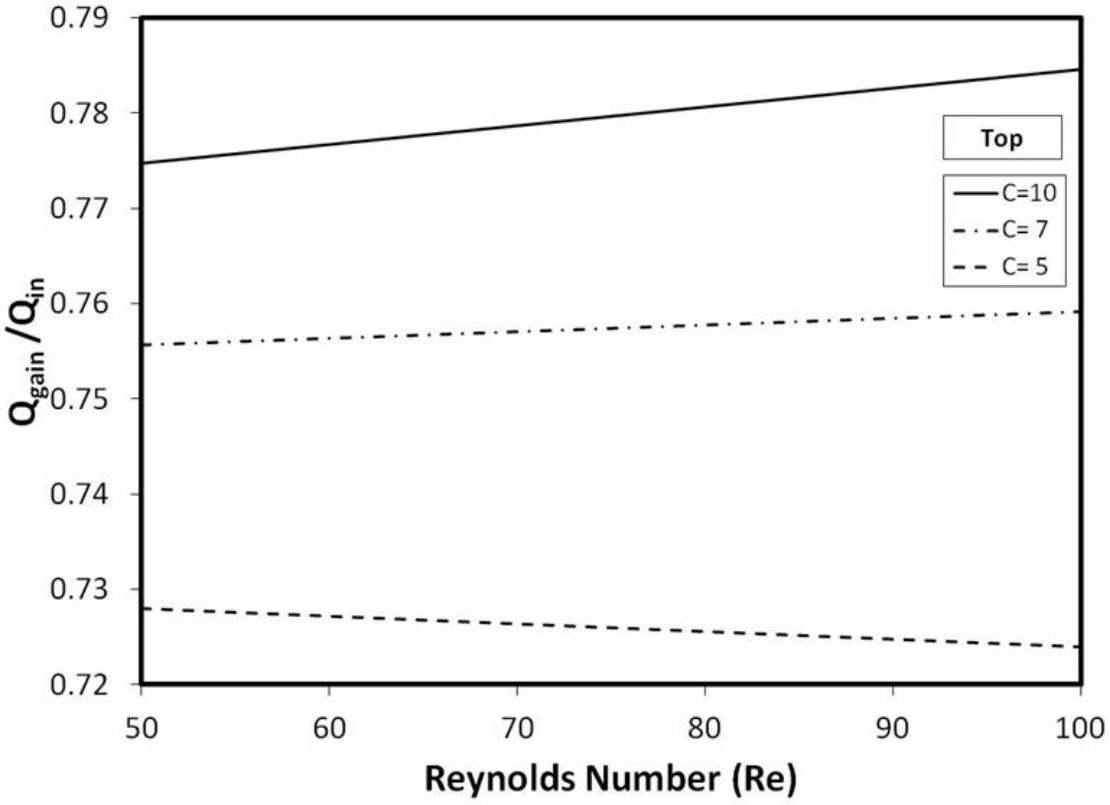

Figure 5.24. Performance parameter variation with Reynolds number for different concentrations. The absorber plate is at the top of the channel.

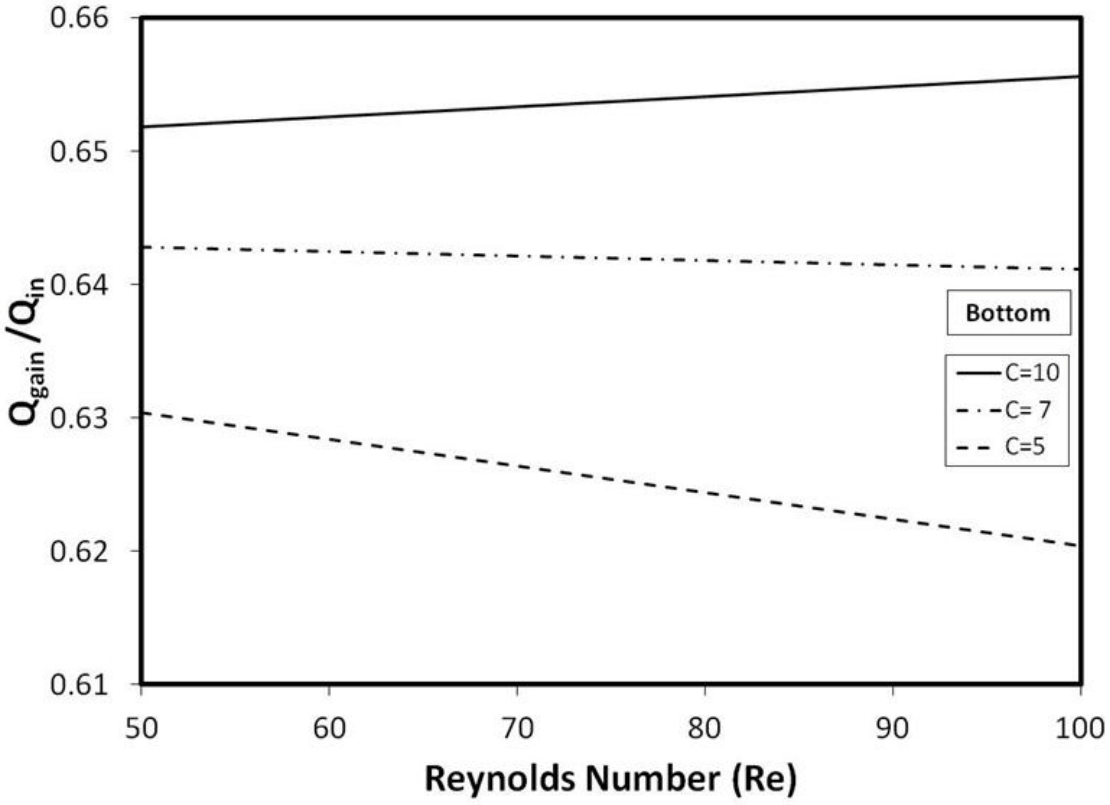

Figure 5.25. Performance parameter variation with Reynolds number for different concentrations. The absorber plate is at the bottom of the channel.

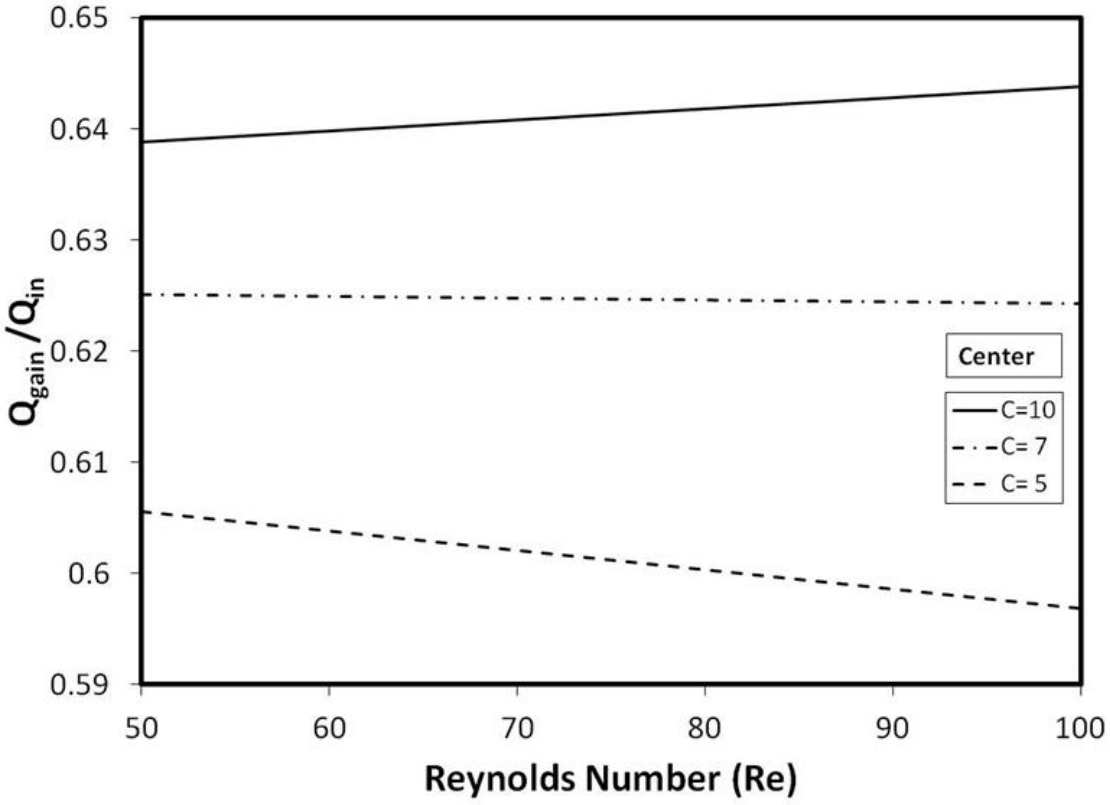

Figure 5.26. Performance parameter variation with Reynolds number for different concentrations. The absorber plate is at the bottom of the channel and 50% transmitted absorber at the mid-height of the channel.

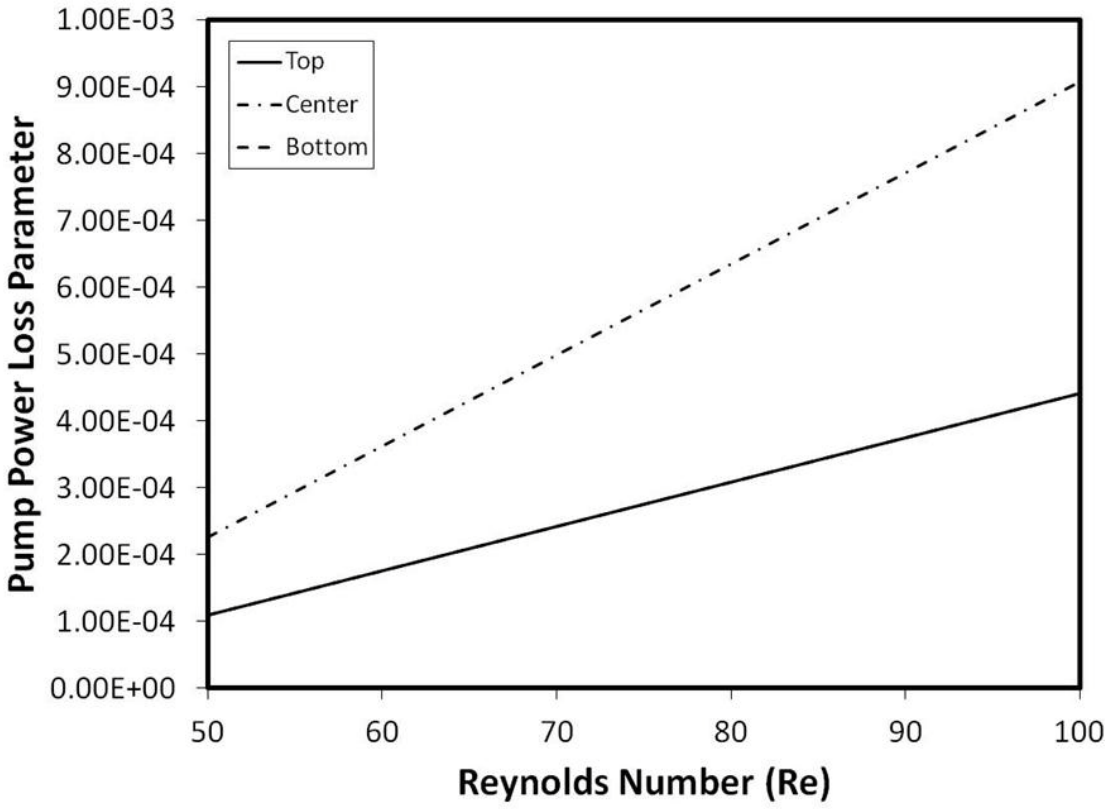

Figure 5.27. Pump power loss parameter variation with Reynolds number for different concentrations and different absorber plate locations in the channel.

CHAPTER 6

CONCLUSION AND FUTURE WORK

This chapter is divided into four sections. In the first three sections, concluding remarks on results in previous chapter are presented. In the last section, some directions are given in which this work can be extended.

6.1 Absorber plate configuration

Thermal performance of solar absorption heating system using the absorbing plate in the horizontal channel is examined. The location of the absorbing plate in the channel is varied and the performance characteristics including performance parameter and the pump power loss parameter are obtained for various Reynolds numbers. In the analysis, energy equation incorporating the full radiation heat transfer is used with the appropriate boundary conditions. In order to validate the model developed, the previous analysis presented for the solar absorption in a channel flow is simulated incorporating the identical boundary conditions. It is found that model predictions agree well the findings of the previous study. Bulk fluid temperature attains high values for the absorbing plate location at the center of the channel. Increasing Reynolds number lowers bulk fluid temperature in the channel, which is more pronounced at high Reynolds numbers. The

performance parameter (Q_{gain}/Q_{in}) increases with increasing Reynolds number, which is associated with the high mass flow rate at high Reynolds numbers. Increasing solar concentration has significant effect on the performance parameter; in which case, performance parameter increases notably at high solar concentrations. The performance parameter varies with the location of absorbing plate in the channel. In the case of low solar concentration (C = 1), the absorbing plate at mid-height of the channel results in the highest performance parameter. However, this changes at high solar concentration (C = 5); in which case, the performance parameter attains the highest value for absorbing plate location at the top of the channel. The pump power parameter increases with increasing Reynolds number due to increased frictional losses in the channel. In addition, the pump power loss parameter attains the highest value for the absorbing plate location at the mid-height of the channel.

6.2 Low Reynolds Number with P.C.M. Particles

Thermal performance characteristics of volumetric solar absorption flow system including absorbing plate in the channel are investigated. Absorber plate consists of a selective surface, which is made from ZrN coating at the silver thin plate surface. In order to enhance the heat storage capacity of the working fluid, the phase change particles consisting of lauric acid is incorporated in the analysis. The study is extended to include the influence of the Reynolds number on the performance and pump power loss parameters for different locations of the absorber plate in the channel. It is found that the performance parameter, which is defined as the thermal energy gain over the solar heat input, is higher for the absorber plate location at the bottom surface of the channel as

compared to those corresponding to the top and mid-height of the channel. This is attributed to the increased fluid bulk temperature due to convection, conduction, and radiation heat transfer from the absorber plate to the working fluid as well as absorption of the incident solar radiation by the fluid. The presence of phase change particles influences the thermal energy storage capacity of the working fluid; in which case, the performance parameter increases considerably as compared to that corresponding to water only. Increasing Reynolds number increases the performance parameter significantly, which is attributed to heat transfer due to forced convection. The pump power loss parameter behaves similar for the absorbing plate location at the top and at the bottom of the channel. However, it increases almost double of its value for the absorber plate locations at the mid-height of the channel due to pressure loss.

6.3 High Reynolds Number with P.C.M. Particles

The performance characteristics of volumetric solar absorber consisting of an absorber plate and channel flow are simulated for different solar concentrations and Reynolds numbers. In order to improve thermal storage capacity of the working fluid, phase change particles at 7% volume concentration is incorporated in the carrier fluid. Lauric acid is used as phase change particles and water is the carrier fluid. The absorber plate consists of ZrN thin coating (16 μm) onto a silver plate. The influence of absorbing plate location on the heat transfer is also examined in the channel. It is found that the Nusselt number along the absorber plate surface increases considerably with the absorber plate location at the mid-height of the channel. This is attributed to the behavior of phase change process in the neighborhood of the absorber plate surface. Although solar absorption and

scattering of working fluid is incorporated in the radiation model, the significant amount of absorption takes place at the absorbing plate in the channel. Increasing Reynolds number modifies slightly the Nusselt number behavior along the absorber plate surface. In this case, the phase change process extends over the length of the absorber plate surface at high Reynolds number. The performance parameter increases almost linearly with increasing Reynolds number; however, the change in concentration alters this behavior. Therefore, the performance parameter reduces with increasing Reynolds number at low concentration, which is true for the absorber plate location at the mid-height and at the bottom of the channel. The performance parameter is the highest for the absorber plate location at the top surface of the channel. Consequently, operating the volumetric solar absorption system at high Reynolds number for absorber plate location at the top of the channel provides improved thermal energy gain, which is more pronounced at high concentrations. The pump power loss parameter increases significantly for the absorber plate location at the mid-height of the channel.

6.4 Future Work

The flow behavior through three geometric channels is considered with different positions of the absorbing surface. There are certain directions in which this work can be extended.

The center absorber was taken at the mid-height of the channel. Its position can be altered by moving it upwards or downwards. It would affect the results as seen from Figure 5.11,

where the bulk temperature at the top section of the channel is lower than the lower section. By moving the plate down, much more uniform temperature can be achieved.

The addition of Lauric acid particles decreased the thermal conduction of the fluid. Particles with higher thermal conductivity like Alumina particles may be added to increase the thermal conductivity of the slurry.

NOMENCLATURE

a	absorption coefficient [m^{-1}]
A	irradiated area [m^2]
CE	conversion efficiency
C	solar concentration
c	volume concentration of nano particles
c_p	specific heat [J kg^{-1} K^{-1}]
$c_{p,S}$	specific heat of particles in solid state[J kg^{-1} K^{-1}]
$c_{p,L}$	specific heat of particles in liquid state [J kg^{-1} K^{-1}]
D_h	hydraulic diameter channel [m]
E	performance parameter
f_d	diffuse fraction
h	heat transfer coefficient [W m^{-2} K^{-1}]
h_L	pump power loss parameter
$h_{p,L}$	pump power loss [Pa]
I	incident radiation intensity [W m^{-2}]
k	thermal conductivity [W m^{-1} K^{-1}]
L_{fusion}	latent heat of fusion of P.C.M. particles [J kg^{-1}]
$\dot{m}$	mass flow rate [kg s^{-1}]
n	refractive index

Nu	Nusselt number
p	pressure [Pa]
Pe	Peclet number
Pr	Prandtl number
ΔP	pressure loss in the channel [Pa]
$q"$	heat flux [W m^{-2}]
Q_a	absorbed solar flux [W m^{-2}]
Q_e	emitted flux [W m^{-2}]
Q_{gain}	energy gained by the fluid [W]
Q_{in}	incident energy [W]
Q_s	incoming solar flux
Re	Reynolds number
S	energy source term
T	local temperature [K]
T_b	bulk fluid temperature [K]
T_{in}	temperature at inlet of control volume [K]
T_{max}	maximum local temperature [K]
T_{out}	temperature at exit of control volume [K]
$T_{solidus}$	lower melting temperature [K]
$T_{liquidus}$	upper melting temperature [K]
T_w	wall temperature [K]

v	velocity [m s^{-1}]
$\dot{V}$	volume flow rate [m^3 s^{-1}]

Greek Symbols

ε_w	wall emissivity
ϕ	temperature ratio
ρ	density [kg m^{-3}]
σ	Stefan-Boltzmann constant
μ	dynamic viscosity [N s m^{-2}]

Subscripts

b	bulk fluid
f	carrier fluid
p	particle

REFERENCES

[1] L.S. Langston, "*Efficiency by the Numbers http://memagazine.asme.org/Web/Efficiency_by_Numbers.cfm,*" (2009).

[2] M. Romero, R. Buck, J.E. Pacheco, "*An Update on Solar Central Receiver Systems, Projects, and Technologies,*" J. Sol. Energy Eng. 124 (2002) 98.

[3] R. Bertocchi, J. Karni, A. Kribus, "*Experimental evaluation of a non-isothermal high temperature solar particle receiver,*" Energy. 29 (2004) 687–700.

[4] H.H. Klein, R. Rubin, J. Karni, "*Experimental Evaluation of Particle Consumption in a Particle Seeded Solar Receiver,*" J. Sol. Energy Eng. 130 (2008) 011012.

[5] T. Fend, B. Hoffschmidt, R. Pitz-Paal, O. Reutter, P. Rietbrock, "*Porous materials as open volumetric solar receivers: Experimental determination of thermophysical and heat transfer properties,*" Energy. 29 (2004) 823–833.

[6] G. Ravi, "*Study of laminar flow forced convection heat transfer behavior of a phase change material fluid study of laminar flow forced convection heat transfer behavior of a phase change material fluid,*" (2008).

[7] E.M. Mehalick, A.T. Tweedie, "*Two component thermal energy storage material,*" Final Report General Electric Co, PA. Space Div. 1 (1975).

[8] V. Trisaksri, S. Wongwises, "*Critical review of heat transfer characteristics of nanofluids,*" Renewable and Sustainable Energy Reviews. 11 (2007) 512–523.

[9] A. Lenert, E.N. Wang, "*Optimization of nanofluid volumetric receivers for solar thermal energy conversion,*" Solar Energy. 86 (2012) 253–265.

[10] F.. Forson, M. a. . Nazha, H. Rajakaruna, "*Experimental and simulation studies on a single pass, double duct solar air heater,*" Energy Conversion and Management. 44 (2003) 1209–1227.

[11] R. Tyagi, H., Phelan, P. E., and Prasher, "*Predicted Efficiency of a Low-Temperature Nanofluid-Based Direct Absorption Solar Collector,*" J. Sol. Energy Eng. Volume 131 (2009) 041004.

[12] N.P. Nwosu, "*Employing exergy-optimized pin fins in the design of an absorber in a solar air heather,*" Applied Solar Energy. 45 (2010) 248–253.

[13] A. Veeraragavan, A. Lenert, B.S. Yilbas, S. Al-Dini, E.N. Wang, "*Analytical model for the design of volumetric solar flow receivers,*" International Journal of Heat and Mass Transfer. 55 (2012) 556–564.

[14] G. Alvarez, J. Arce, L. Lira, M.R. Heras, "*Thermal performance of an air solar collector with an absorber plate made of recyclable aluminum cans,*" Solar Energy. 77 (2004) 107–113.

[15] Z. Wu, C. Caliot, G. Flamant, Z. Wang, "*Coupled radiation and flow modeling in ceramic foam volumetric solar air receivers,*" Solar Energy. 85 (2011) 2374–2385.

[16] A.A. Hegazy, "*Performance of Flat plate solar air heaters with optimum channel geometry for constant / variable flow operation,*" Energy Conversion and Management. 41 (2000) 401–417.

[17] P. Dhiman, N.S. Thakur, A. Kumar, S. Singh, "*An analytical model to predict the thermal performance of a novel parallel flow packed bed solar air heater,*" Applied Energy. 88 (2011) 2157–2167.

[18] W. Sun, J. Ji, W. He, "*Influence of channel depth on the performance of solar air heaters,*" Energy. 35 (2010) 4201–4207.

[19] P. Promvonge, C. Khanoknaiyakarn, S. Kwankaomeng, C. Thianpong, "*Thermal behavior in solar air heater channel fitted with combined rib and delta-winglet,*" International Communications in Heat and Mass Transfer. 38 (2011) 749–756.

[20] F. Ozgen, M. Esen, H. Esen, "*Experimental investigation of thermal performance of a double-flow solar air heater having aluminium cans,*" Renewable Energy. 34 (2009) 2391–2398.

[21] D.P. Colvin, J.C. Mulligan, "*Spacecraft Heat Rejection Methods: Active and Passive Heat Transfer for Electronic Systems.,*" (1986).

[22] Roy S. K., S. S., "*An evaluation of phase change microcapsules for use in enhanced heat transfer fluids,*" Nternational Communications in Heat and Mass Transfer. 18 (1991) 495–507.

[23] M. Goel, S.K. Roy, S. Sengupta, "*Laminar forced convection heat transfer in microcapsulated phase change material suspensions,*" International Journal of Heat and Mass Transfer. 37 (1994) 593–604.

[24] P. Charunyakorn, S. Sengupta, S.K. Roy, "*Forced convection heat transfer in microencapsulated phase change material slurries : flow in circular ducts,*" Int. J. Heat Mass Transfer. 33 (1990) 819–833.

[25] E. Choi, Y.I.. Cho, H.G. Lorsch, "*Forced convection heat transfer with phase-change-material slurries: Turbulent flow in circular tube,*" International Journal of Heat and Mass Transfer. 37 (1994) 207–215.

[26] Y. Zhang, A. Faghri, "*Analysis of forced convection heat transfer in microencapsulated phase change material suspensions,*" Journal of Thermophysics and Heat Transfer. 9 (1995) 727–732.

[27] S.K. Roy, B.L. Avanic, "*Laminar Forced Convection Heat Transfer With Phase Change Material Emulsions,*" Int. Comm. Heat Mass Transfer. 24 (1997) 653–662.

[28] E.L. Alisetti, S.K. Roy, "*Forced Convection Heat Transfer to Phase Change Material Slurries in Circular Ducts,*" J. Thermophysics. 14 (1999) 115–118.

[29] Y. Yamagishi, H. Takeuchi, A.T. Pyatenko, N. Kayukawa, "*Characteristics of microencapsulated PCM slurry as a heat-transfer fluid,*" AichE Journal. 45 (1999) 696–707.

[30] S.K. Roy, B.L. Avanic, "*Laminar Forced Convection Heat Transfer with Phase Change Material Suspensions,*" Int. Comm. Heat Mass Transfer. 28 (2001) 895–904.

[31] X. Hu, Y. Zhang, "*Novel insight and numerical analysis of convective heat transfer enhancement with microencapsulated phase change material slurries: laminar flow in a circular tube with constant heat flux,*" International Journal of Heat and Mass Transfer. 45 (2002) 3163–3172.

[32] A.B.S. Alquaity, S.A. Al-Dini, E.N. Wang, S.Z. Shuja, K.J.S. B.S. Yilbas, "*Heat Transfer Enhancement in Microchannel Flow: Presence of Microparticles in a Fluid,*" in: Proceedings of the 8th International Conference on Nanochannels, Montreal, Canada, 2011: pp. 353–358.

[33] R. Blickensderfer, "*Solar Absorbers—Selective Surfaces,*" in: Electric Refractory Materials, 2000.

[34] F. Mammadov, "*Study of Selective Surface of Solar Heat Receiver,*" International Journal of Energy Engineering. 2 (2012) 138–144.

[35] "*Product Documentation, Fluent 12.1., ANSYS Inc. http://www.sharcnet.ca/Software/Fluent12/index.htm,*" (n.d.).

[36] A.B.S. Alquaity, *Modeling of thermal performance of liquid flow with nanosized particles of phase change material in microchannels, King Fahad University of Petroleum and Minerals, 2011*.

[37] J.C. Maxwell, "*A Treatise on Electricity and Magnetism,*" Dover Publications, New York., 1954.

[38] V. V. Vand, "*Theory of viscosity of concentrated suspensions,*" Nature. 155 (1945) 364–365.

[39] R. Sabbah, M.M. Farid, S. Al-Hallaj, "*Micro-channel heat sink with slurry of water with micro-encapsulated phase change material: 3D-numerical study,*" Applied Thermal Engineering. 29 (2008) 445–454.

[40] S. V. Patankar, "*Numerical heat transfer and fluid flow,*" Hemisphere Publishing Corporation, 1980.

[41] K.Q. Xing, "*Performance Evaluation of Liquid Flow With PCM Particles in Microchannels,*" Journal of Heat Transfer. 127 (2005) 931–940.

[42] G. Yamamoto, G. Ünishi, "*Absorption of solar radiation by water vapor in atmosphere,*" Journal of Meteorology. 9 (1952) 415–421.

VITA

Name: Osman Kaleem Siddiqui

Date of Birth: December 9, 1987

Present Address: KFUPM P. O. Box 8593, King Fahd University of Petroleum and Mineral, Dhahran-31261, Saudi Arabia

Permanent Address: House No. 40, Mehran Block, Allama Iqbal Town, Lahore, Pakistan

Email Address: osmankaleem@kfupm.edu.sa

osmankaleem@hotmail.com

Telephone: + 966 551 328460

Educational Qualification:

M.S (Mechanical Engineering)

May, 2013

King Fahd University of Petroleum & Minerals,

Dhahran, Saudi Arabia.

B.Sc. (Mechanical Engineering)

August, 2009

University of Engineering and Technology

Lahore, Pakistan.